



HAL
open science

Nonlocal thermal diffusion in one-dimensional periodic lattice

Vincent Picandet, Noël Challamel

► **To cite this version:**

Vincent Picandet, Noël Challamel. Nonlocal thermal diffusion in one-dimensional periodic lattice. *International Journal of Heat and Mass Transfer*, 2021, 180, pp.121753. 10.1016/j.ijheatmasstransfer.2021.121753 . hal-04832143

HAL Id: hal-04832143

<https://hal.science/hal-04832143v1>

Submitted on 19 Dec 2024

HAL is a multi-disciplinary open access archive for the deposit and dissemination of scientific research documents, whether they are published or not. The documents may come from teaching and research institutions in France or abroad, or from public or private research centers.

L'archive ouverte pluridisciplinaire **HAL**, est destinée au dépôt et à la diffusion de documents scientifiques de niveau recherche, publiés ou non, émanant des établissements d'enseignement et de recherche français ou étrangers, des laboratoires publics ou privés.



Distributed under a Creative Commons Attribution - NonCommercial 4.0 International License

Nonlocal thermal diffusion in one-dimensional periodical lattice

Vincent Picandet and Noël Challamel

Université Bretagne-Sud, IRDL, UMR CNRS 3744, F-56100 Lorient, France

1 Abstract

2 *Heat conduction in micro-structured rods can be simulated with unidimensional*
3 *periodical lattices. In this paper, scale effects in conduction problems, and more*
4 *generally in diffusion problems, are studied from a one-dimensional thermal lattice.*
5 *The thermal lattice is governed by a mixed differential-difference equation, accounting*
6 *for some spatial microstructure. Exact solutions of the linear time-dependent spatial*
7 *difference equation are derived for a thermal lattice under initial uniform temperature*
8 *field with some temperature perturbations at the boundary. This discrete heat equation*
9 *is approximated by a continuous nonlocal heat equation built by continualization of*
10 *the thermal lattice equations. It is shown that such a nonlocal heat equation may be*
11 *equivalently obtained from a nonlocal Fourier's law. Exact solutions of the thermal*
12 *lattice problem (discrete heat equation) are compared with the ones of the local and*
13 *nonlocal heat equation. An error analysis confirms the accurate calibration of the*
14 *length scale of the nonlocal diffusion law with respect to the lattice spacing. The*
15 *nonlocal heat equation may efficiently capture scale effect phenomena in periodical*
16 *thermal lattices.*

17

18 *Key words: Nonlocality, Diffusion equation, Gradient Fourier's law, Heat equation,*
19 *Lattice.*

20

21 1. Introduction

22

23 This paper explores the possibility to characterize the thermal behaviour of
24 heterogeneous one-dimensional medium with a nonlocal approach, based on the
25 introduction of some scale effects in the nonlocal diffusion model. A thermal lattice
26 will be studied from a mixed differential-difference equation that will be analytically
27 solved. The second part of the paper is devoted to the continuous approaches that may
28 be valid to capture the scale effects inherent to the lattice properties. Scale effects may
29 be predominant for engineering applications at different scales, from nanoscale

30 structures to macro-structures, where the size of unit cell may play some significant
 31 roles.

32

33 The behaviour of a basic periodical thermal lattice with direct thermal interactions,
 34 fully described in section 2.1, is explored. Such discrete media is based on a physical
 35 thermal lattice ruled by a mixed difference differential equation, see [1]:

$$T_i' = \alpha \frac{T_{i+1} - 2T_i + T_{i-1}}{a} \quad (1)$$

36 where T_i is the temperature at the node i and T_i' denotes its time derivative, α is the
 37 thermal diffusivity and a is the lattice spacing due to the discreteness of the discrete
 38 thermal system. $T_i(t)$ is discrete temperature field which is continuous in time at node i .
 39 Such a lattice has been already considered, for instance with exact time-dependent
 40 solutions for initial conditions defined as hat-function [2]. Eq. (1) is continuous in time
 41 and discrete in space due to the lattice spacing. It can be also viewed as a discrete heat
 42 equation in space. Zingales [3] studied the behaviour of an inhomogeneous thermal
 43 lattice with spatial dependent thermal conductivity and specific heat coefficients.

44

45 The aim of the present paper is to investigate the capability of some nonlocal heat
 46 partial differential equations to capture the inherent scale effects into such periodical
 47 thermal lattice system. A nonlocal heat equation can be built from continualization of
 48 the thermal lattice system, using asymptotic expansion of the associated pseudo-
 49 differential operator. The nonlocal heat equation is augmented by some coupled spatial
 50 and time-dependent terms which are affected by the lattice parameters:

$$T' = \alpha T'' + l_c^2 T'' \quad \text{with } l_c^2 = a^2 / 12 \quad (2)$$

51 Eq. (2) is a nonlocal heat diffusion equation which can be also classified as a Guyer-
 52 Krumhansl equation [4] [5] (see for instance [2] [6] [7] or [8] for analytical solutions of
 53 such an equation). As a simplification, we neglect in this study some additional
 54 viscous terms specific of the Cattaneo-Vernotte model [9]. We show that the efficiency
 55 of this continuous nonlocal heat model to capture the scale effects strongly depends on
 56 the continualization of both the discrete field and the discrete initial conditions. It also
 57 depends on the considered time during the evolution process as the continualization
 58 process involves time and spatial coupling effects. Exact solutions will be derived for

59 both systems, the discrete one ruled by a discrete Fourier summation, and the nonlocal
60 continuous one governed by a continuous Fourier series formulation.

61

62 Since the energy balance equation may be written as:

$$\rho C T' = -\varphi' \quad (3)$$

63 where φ is the heat flux density, ρ is the density and C is the specific heat capacity of
64 the rod, the considered nonlocal heat equation given into Eq. (2) leads to a nonlocal
65 one-dimensional Fourier's law:

$$\varphi - l_c^2 \varphi'' = -\kappa T' \quad (4)$$

66 where, κ is thermal conductivity (with $\kappa = \alpha \rho C$), and l_c is the characteristic length of
67 the nonlocal model containing the microstructure information due to its periodical
68 discreteness. It is worth to note that this differential nonlocal Fourier's law is
69 mathematically similar to the differential nonlocal model introduced by Eringen [10]
70 for nonlocal elasticity models, using a similar differential implicit law between the
71 stress and the strain.

72

73 Such nonlocal diffusion equation has been already considered for mass-transfer
74 modeling by Barenblatt [11] applied to liquid flows in cracked rocks, and more
75 recently in heat diffusion in the same periodically micro structured rod [2]. Exact
76 solutions of this nonlocal heat equation have been derived for various initial and
77 boundary conditions [2] [11] [12].

78

79 Nonlocal diffusion problems have been also studied by many authors, with an
80 additional characteristic time making this equation both non local in time and space
81 [13] [14] [15] [16] [17] [18] [19] [20] [21] [22]. The nonlocal Fourier's law is an
82 evolution equation of Guyer-Krumhansl type which relates the heat flux with respect
83 to the temperature field using an additional length scale for the flux. For the complete
84 Guyer-Krumhansl type model, an additional relaxation time (as for Cattaneo's model)
85 has to be considered in addition to the spatial nonlocal length scale, see [4] [5] [6] [23].

86

87 Thermal lattices have been already studied in the literature, from a thermal random
88 walk process connected with partial differential equations [24]. Weymann (1967) [25]
89 and Taitel (1972) [26] have characterized such discrete diffusion by a coupled spatial-
90 time difference equation leading to higher-order gradient heat equation and have
91 looked for the possibility to treat this lattice difference equation from some extended
92 partial differential equations using higher-order gradient operators as an approximation
93 of the initial discrete problem. The expansion of the associated time and spatial
94 pseudodifferential operators using Taylor asymptotic expansion, gives higher-order
95 time and spatial derivatives in the heat equation. The same methodology has been
96 followed by Sobolev (1992, 2014) [27] [28] for the same thermal random walk
97 equation, see more recently [29]. The methodology presented in this paper is not so
98 far, even if the initial thermal lattice equation considered in this paper slightly differs
99 from the random walk equation, in the sense that the time evolution remains local for
100 the temperature variable (we only take into account spatial microstructures).

101

102 In this study, the exact resolution of the mixed differential-difference heat equation,
103 valid for the thermal lattice (which may also cover other discrete diffusion processes)
104 is presented. A nonlocal continuous approximation of this lattice model is thought,
105 using a Padé approximant of the spatial pseudo-differential operator, thus avoiding
106 higher-order spatial derivatives. The nonlocal heat equation finally uses coupled
107 continuous spatial and time derivatives.

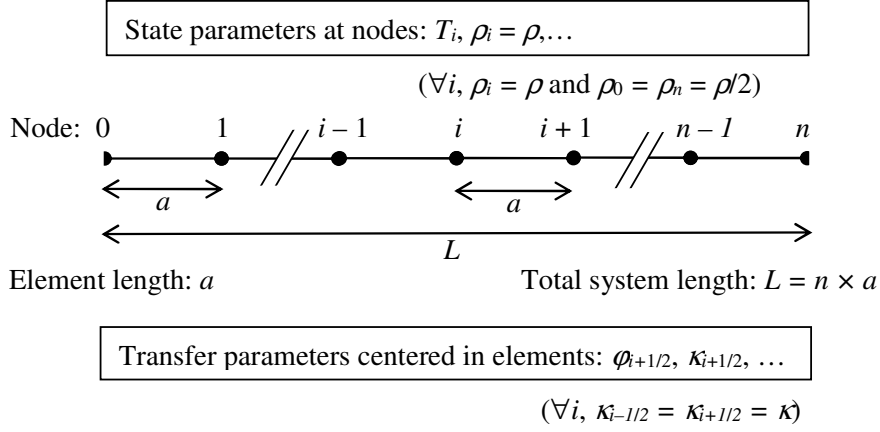
108

109 **2. Thermal discrete lattice.**

110 *2.1. Definition*

111 The physical discreteness of the material can be assumed at least at the atomic scale.
112 Other heterogeneities at larger scales can also be considered. In this study, a periodic
113 discrete lattice is assumed, consisting in n rigid elements with a constant length equal
114 to $a = L/n$, as already studied by the authors [2] and, with additional heterogeneities by
115 Zingales [3].

116



117
118
119

Fig. 1 : Periodic thermal lattice of n elements-chain

120 The discrete-based (or lattice) approach is schematically presented in Fig. 1. Here, the
121 state parameters as masses, equal to $a\rho_i$ or temperature T_i are located at each node.
122 Half common node masses are associated to both edge nodes so the total weight of the
123 whole chain is equal to ρL , as for discrete chains already studied through mechanical
124 aspects and vibration problems [30]. Here, this consideration has no incidence on heat
125 diffusion, since the temperature is imposed at both edge nodes. The transfer parameters
126 as heat flux, $q_{i+1/2}$, and thermal conductivity $\kappa_{i+1/2}$, are defined at the interval between
127 nodes and considered as centered into the conductive elements. Based on the following
128 spatially discrete Fourier's law the associated energy balance gives:

$$\varphi_{i+1/2} = -\kappa_{i+1/2} \frac{T_{i+1} - T_i}{a} \text{ and } \rho C T_i \dot{\&} = -\frac{\varphi_{i+1/2} - \varphi_{i-1/2}}{a} \quad (5)$$

129 The discrete heat diffusion equation can then be formulated as Eq. (1). This mixed
130 difference-differential equation slightly differs from the difference equation in space
131 and in time studied by Taitel from a thermal random walk equation [26].

132

133 The aim of this study is to focus on time evolution of temperature into this finite
134 discrete rod, initially at stable and constant temperature T_{ini} and disturbed at $t = 0$ with
135 the same imposed temperature at both ends T_{imp} , with $T_{imp} \neq T_{ini}$, remaining constant
136 for $t > 0$. Thereafter, the normalized dimensionless temperature, \bar{T} , is considered

$$\bar{T} = 1 - \frac{T_{imp} - T}{T_{imp} - T_{ini}} = \frac{T - T_{ini}}{\Delta T} \text{ with } \Delta T = T_{imp} - T_{ini} \neq 0 \quad (6)$$

137

138 The following dimensionless parameters, normalized with respect to the physical
 139 characteristics of the rod, L and α are introduced. They correspond to longitudinal
 140 coordinate, x^* , and the elapsed time after the imposed change in temperature at
 141 boundaries, t^* , and the normalized heat flux density $\bar{\varphi}$ such as:

$$x^* = \frac{x}{L} \text{ or } x_i^* = \frac{i}{n} \text{ in case of discrete lattice;}$$

$$t^* = \frac{\alpha t}{L^2} \text{ with } \alpha = \frac{\kappa}{\rho C} \text{ such as } \bar{T}' = \frac{\partial \bar{T}}{\partial t^*} = \frac{1}{\Delta T} \frac{\partial T}{\partial t^*} = \frac{L^2}{\alpha \Delta T} \frac{\partial T}{\partial t} \text{ and}$$

$$\bar{\varphi} = \frac{L}{\Delta T} \frac{\varphi}{\kappa} \text{ such as Eq.(1) gives } \bar{\varphi}' = \frac{L^2}{\Delta T} \frac{\varphi'}{\kappa} = \frac{L^2}{\alpha \Delta T} \frac{\varphi'}{\rho C} = -\frac{\partial \bar{T}}{\partial t^*} = -\dot{\bar{T}}$$
(7)

142
 143 The dimensionless discrete heat diffusion equation of the thermal lattice can then be
 144 reformulated from Eq. (1), as:

$$\bar{T}'_i = n^2 (\bar{T}_{i+1} - 2\bar{T}_i + \bar{T}_{i-1})$$
(8)

145
 146 The local difference equation of the thermal lattice system (with $l_c = 0$) has been
 147 widely studied through numerical treatments using time and spatial discretization, for
 148 instance in [31] [32], [33] and more recently in [34]. In this paper, it should be noted
 149 that local difference equation of the thermal lattice exactly matches the finite-
 150 difference formulation of the one-dimensional heat diffusion equation with a
 151 continuous time parameter.

152 2.2. Exact solution of the thermal lattice difference equation

153 As for the classical resolution of the local heat equation, the method of separation of
 154 continuous time and discrete space variables, based on $\bar{T}_i(t^*) = \xi_i \tau(t^*)$, where \bar{T}_i is
 155 the dimensionless temperature at node i , leads to:

$$\frac{\bar{T}'_i}{\tau} = n^2 \frac{\xi_{i+1} - 2\xi_i + \xi_{i-1}}{\xi_i} \text{ with } \bar{T}'_i = \frac{d\tau}{dt^*}$$
(9)

156
 157 The time dependent term, $\tau(t^*)$, can be first easily integrated: $\tau = P_1 \exp(-\gamma t^*)$ where
 158 P_1 is a constant parameter. Then, a linear second-order difference equation in space

159 remains. The homogeneous linear second-order difference with constant coefficients
 160 may be solved if a power law function is introduced [35] , i.e. $\xi_i = \xi \lambda^i$, see for instance
 161 [36], giving the auxiliary equation according to λ :

$$\xi_{i+1} + \left(\frac{\gamma}{n^2} - 2 \right) \xi_i + \xi_{i-1} = 0 \text{ leads to } \lambda + \frac{1}{\lambda} = 2 - \frac{\gamma}{n^2} \quad (10)$$

162

163 Eq. (10) is symmetrical with respect to interchanging λ and $1/\lambda$. This equation admits
 164 the two complex solutions λ_1 and λ_2 for $0 < \gamma/n^2 < 4$, i.e. if $|1 - \gamma/2n^2| < 1$:

$$\lambda_{1,2} = \cos(\phi) \pm j \sin(\phi) \text{ with } \phi = \arccos(1 - \gamma/2n^2) \text{ and } j = \sqrt{-1} \quad (11)$$

165

166 In real basis, the solution of the finite difference equation can be written as:
 167 $\xi_i = P_2 \sin(\phi_i) + P_3 \cos(\phi_i)$ where P_2 and P_3 are constant parameters. From the boundary
 168 conditions: $\bar{T}_0(t^*) = \bar{T}_n(t^*) = 0$ which are equivalent to $\xi_0 = \xi_n = 0$, the solution of ξ_i
 169 can be written as:

$$\xi_i = P_2 \sin\left(\frac{k\pi i}{n}\right) = P_2 \sin(k\pi x_i^*) \quad (12)$$

170 where k is a positive integer. Introducing $\phi = m\pi/n$ into $\phi = \arccos(1 - \gamma/2n^2)$ leads to
 171 $\gamma = 4n^2 \sin^2(m\pi/2n)$. The exact solution of temperature evolution at nodes is then
 172 defined as a discrete Fourier summation:

$$\bar{T}_{i,exact}(x_i^*, t^*) = \sum_{k=1}^{n-1} A_k \sin\left(k\pi \frac{i}{n}\right) \exp\left[-4n^2 \sin^2(k\pi/2n) t^*\right] \quad (13)$$

173

174 where A_k are the discrete Fourier summation coefficients depending on the initial
 175 conditions, inspired from the classical Heaviside initial temperature distribution:

$$\begin{aligned} \text{if } t = 0, T_i(0) = T_{ini} = T_{imp} + \Delta T, \text{ i.e. } \forall i \in [0, n], \bar{T}_i = 1 \text{ and} \\ \text{if } t \geq 0, T_0(t) = T_n(t) = T_{imp}, \text{ i.e. } \bar{T}_0(t^*) = \bar{T}_n(t^*) = 0 \end{aligned} \quad (14)$$

176 These conditions leads to: $A_k = (2/n) \sum_{p=1}^{n-1} \sin(k\pi p/n)$ [37]. The double summation
 177 obtained from injection of A_k into Eq. (13) can be also turned into a single finite
 178 summation, see Appendix A, for a faster and accurate computation:

$$\bar{T}_{i,exact}(x_i^*, t^*) = \frac{1}{n} \sum_{k=1}^{n-1} \frac{1 - (-1)^k}{\tan(k\pi/2n)} \sin\left(k\pi \frac{i}{n}\right) \exp[-4n^2 \sin^2(k\pi/2n) t^*] \quad (15)$$

179

180 Hereafter, this solution is used as a reference at node 1 or $(n-1)$ and the mid node $(n/2)$
 181 to compare the results obtained from continualized model.

182

183 3. Nonlocal continuous heat equation

184

185 3.1. Boundary conditions of equivalent continuous media

186 The key point is the consideration of a disturbance of the discrete temperature field at
 187 both ends of the finite discrete rod. In this study, we will explore the capability of
 188 continuous nonlocal heat equation to capture some scale effects of such discrete
 189 thermal lattices. For the continuous approach, the full definition of the temperature
 190 field is needed within all the bar. Many continualized initial temperature fields built
 191 from a homogeneous initial discrete temperature can be assumed from homogeneous
 192 initial discrete temperature.

193

194 We will consider four basic assumptions about initial continuous field of temperature,
 195 according to $x^* = x/L$, in the continualized nonlocal chain. These assumptions on the
 196 discrete case are transposed from a finite continuous rod, initially at stable and
 197 constant temperature T_0 and disturbed at $t = 0$ with the same temperature imposed at
 198 both ends. The initial and boundary conditions of equivalent continuous media are:

$$\begin{aligned} \text{if } t = 0, \forall x^* \in]0;1[, \bar{T}(x^*, 0) = 1 \text{ in "Heaviside" case,} \\ \forall x^* \in [1/n; 1-1/n], \bar{T}(x^*, 0) = 1 \text{ in other cases} \end{aligned} \quad (16)$$

$$\text{if } t \geq 0, \bar{T}_0(0, t^*) = \bar{T}_n(1, t^*) = 0$$

199

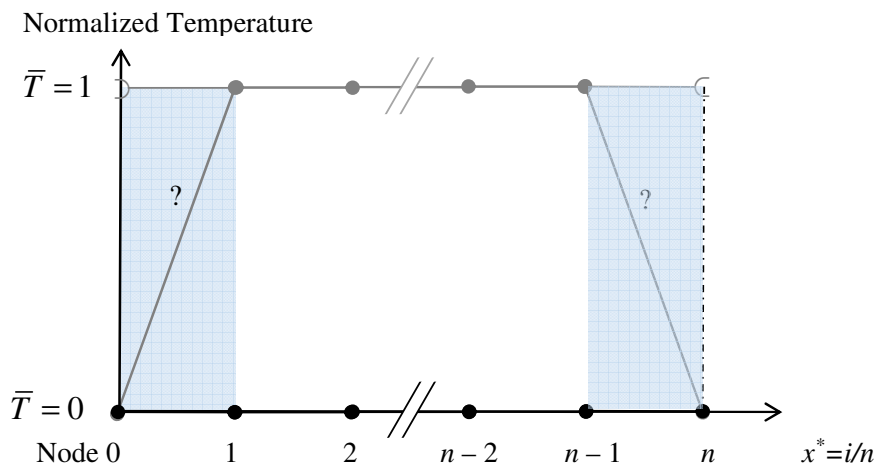
200 In the continuous case, the initial temperature (at $t = 0$) corresponds to a step function
 201 located at both ends, made of a combination of Heaviside functions, discontinuous in
 202 time and space.

203

204 – The first assumption considers a direct transposition of the continuous case, i.e. the
 205 same initial temperature distribution in the discrete system, even into the edge
 206 elements. This transposition of the discontinuous Heaviside distribution of temperature
 207 to the discrete one assumes a discontinuous time evolution of temperature at both edge
 208 nodes. This assumption on the discrete system, named as “Heaviside” boundary
 209 condition, will be used as a reference thereafter, since it is usually considered to
 210 numerically solve the basic heat equation. However, if a non-null mass is located in
 211 both edge nodes as assumed in discrete system, it is not physically consistent. With
 212 lower values of n , this lead to a paradox at both tip nodes, that have to be set at a
 213 different temperature of the rest of edge (first and last) elements of the chain.
 214 Preliminary studies [38] have shown that such strong discontinuity induces a bias into
 215 the resolution of difference equations and Fourier series as in the continualization
 216 process exposed in the next part.

217

218 In order to avoid discontinuity in time evolution of temperature, the initial distribution
 219 of temperature, at $t = 0$, has to make the edge nodes temperatures already equal to T_{imp} .
 220 To approximate as much as possible the classical Heaviside distribution, the next node
 221 temperature, inward the chain, has to be equal to T_0 . The remaining question is about
 222 initial distribution of temperature into the edge elements, i.e. between the nodes 0 and
 223 1, and the nodes $n-1$ and n , see Fig. 2.



224

225

226

Fig. 2 : Initial distribution of temperature into equivalent continuous media

227 Here after, dimensionless part functions of $\bar{T}(x^*, 0)$ are considered, such as:

$$\begin{aligned}
 \bar{T}(x^*, 0) &= f_{edge}(x^*) \leq 1 && \text{for } x^* \in [0; 1/n] \\
 \bar{T}(x^*, 0) &= 1 && \text{for } x^* \in [1/n; 1-1/n] \\
 \bar{T}(x^*, 0) &= f_{edge}(1-x^*) \leq 1 && \text{for } x^* \in [1-1/n; 1]
 \end{aligned} \tag{17}$$

228

229 – The second assumption assumes an initial distribution of temperature with a constant
 230 gradient, $\Delta T/a$ into both edge elements. Due to the shape of the temperature
 231 distribution according to the longitudinal coordinate, it is name as “trapezoidal”.
 232 However this initial distribution lead to a discontinuous spatial derivative of
 233 temperature at nodes 0 and 1, as well as at nodes $n-1$ and n , that may still induced
 234 bias into nonlocal models.

235

236 – The third assumption, names as “polynomial” assumes an initial distribution of
 237 temperature with a polynomial function of degree p (with $p > 1$) into the edge elements
 238 such as spatial gradient of $T(x^*, 0)$ is null and continuous at the nodes closed the
 239 boundaries, i.e. at the nodes 1 and $n-1$ or at abscissa $x^* = 1/n$ and $x^* = 1-1/n$. The
 240 dimensionless part function of $\bar{T}(x^*, 0)$ in this case is defined by $f_{edge,p}(x^*)$ according
 241 to p as:

$$f_{edge,p}(x^*) = 1 - (1 - nx^*)^p \tag{18}$$

242

243 The “trapezoidal” case corresponds to the case $p = 1$, while the “heaviside” case
 244 corresponds to $p \rightarrow \infty$, see Fig. 3. It should be note that in introduced “polynomial”
 245 functions, the spatial gradient of $T(x^*, 0)$ is discontinuous at the boundaries, in $x^* = 0$
 246 and $x^* = 1$.

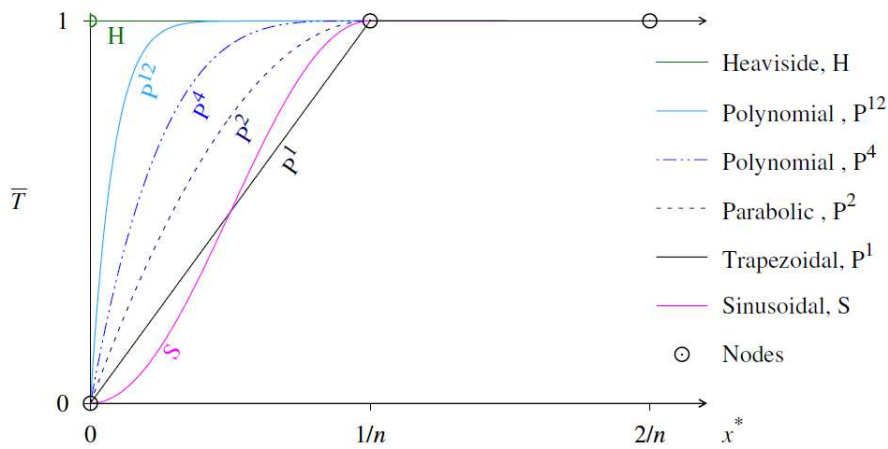
247

248

249 – The fourth assumption, names as “Sinusoidal” is finally introduced in order to ensure
 250 the continuity of the temperature and of its first spatial derivative over the whole
 251 length of the chain. $\bar{T}(x^*, 0)$ and $\partial\bar{T}(x^*, 0)/\partial x^*$ are then continuous at both nodes of
 252 edges elements, i.e. at the nodes 0,1, $n-1$ and n , see Fig. 3. The dimensionless part
 253 function of $\bar{T}(x^*, 0)$ in this case is defined as:

$$f_{edge}(x^*) = \frac{1}{2} [1 - \cos(n\pi x^*)] \quad (19)$$

254



255

256

257

Fig. 3 : Initial temperature distribution into edge elements

258 3.2. Analytical solution of the nonlocal model

259 Following the classical method using the separation of variables, already exposed in
 260 section 2.2, based on $\bar{T}(x, t^*) = \xi(x^*)\tau(t^*)$, the nonlocal heat diffusion equation, see
 261 Eq. (2) can be written in dimensionless form as:

$$\frac{\partial \xi}{\partial x^*} = \frac{\xi''}{\xi} + l_c^{*2} \frac{\xi''}{\xi} \frac{\partial \tau}{\partial t^*} \quad \text{with} \quad \frac{\partial \tau}{\partial t^*} = -\gamma \tau \quad (20)$$

262 For a given continuous abscissa x^* , the first term $\frac{\partial \tau}{\partial t^*}$ remains constant. Assuming
 263 $\frac{\partial \tau}{\partial t^*} = -\gamma$, the following equality is obtained: $\xi''/\xi = \gamma/(l_c^{*2} - 1)$ with $l_c^{*2} < 1/\gamma$. This
 264 last condition about l_c will be discussed later and justified by Eq. (23). The solution of
 265 $\tau(t^*)$ and $\xi(x^*)$ can then be written:

$$\tau = P_4 \exp(-\gamma t^*) \text{ and } \xi = P_5 \sin(m\pi x^*) + P_6 \cos(m\pi x^*) \quad (21)$$

266 where P_4 , P_5 and P_6 are constant parameters to be determined according the initial
 267 boundary conditions, given into Eq. (16) and equivalent to $\xi(0) = \xi(1) = 0$. As a
 268 consequence, the constant parameter P_6 in Eq. (21) is null and $\xi(x^*)$ reduces to:

$$\xi(x^*) = P_5 \sin(m\pi x^*) \quad (22)$$

269 where m is a positive integer. Substitution of ξ''/ξ by $(m\pi)^2$ gives:

$$\gamma = \frac{(m\pi)^2}{1 + l_c^{*2} (m\pi)^2} \quad (23)$$

270 This equation assumes a positive value of γ , and in accordance with the inequality
 271 previously assumed to set the Eq. (21), it can be checked that $0 < \gamma < 1/l_c^{*2}$ whatever
 272 the value of m .

273

274 The solution is obtained through Fourier series for a continuous abscissa x^* :

$$\bar{T}(x^*, t^*) = \sum_{m=1}^{\infty} A_m \sin(m\pi x^*) \exp\left(\frac{-m^2 \pi^2 t^*}{1 + m^2 \pi^2 l_c^{*2}}\right) \quad (24)$$

275

276 where A_m are the continuous Fourier series coefficients defined according the initial
 277 continuous conditions given into Eq. (17) i.e. according to $f_{edge}(x^*)$. the Fourier series
 278 coefficients are all presented in Appendix A.

279

280 It should be noted that the nonlocal solution in Eq. (24) leads to the classical well-
 281 known local solution if the characteristic length, l_c , is null i.e., when $n \rightarrow \infty$. This
 282 solution is also compared to compared to numerical ones based on the resolution of the
 283 local and nonlocal heat differential equation according to the characteristic length, l_c .
 284 The semi-implicit resolution method used and relative details are given in Appendix B.

285

286 As already observed for A_k in section 2.2, the coefficient A_m are always null for even
 287 values of m . Hence, the Fourier series can be expressed and computed more efficiently
 288 with summation of odd values only of harmonics, m .

289 3.3. Extrapolation of the lattice exact solution

290 The discrete solution at the nodes of the lattice given into Eq. (13) can also be
291 extended as a continuous solution using the same integration over the whole length of
292 the chain to determine the A_m coefficients of Fourier series:

$$\bar{T}_{exact}(x^*, t^*) = \sum_{m=1}^{\infty} A_{2m-1} \sin[(2m-1)\pi x^*] \exp\left[-4n^2 \sin^2\left(\frac{(2m-1)\pi}{2n}\right) t^*\right] \quad (25)$$

293

294 The extended exact solutions computed from this equation are plotted through the
295 continuous abscissa x^* between the nodes in Fig. 4 *a*) and *b*). Whatever the continuous
296 initial distribution of temperature, the node temperatures converge rapidly toward the
297 same solution given by Eq. (13), matching exactly the lattice temperature at the node
298 abscissa, i.e. for $x^* = x_i^* = i/n$. These analytical results are checked with numerical
299 ones. The numerical finite difference scheme used and more details are presented in
300 Appendix B.

301

302 As a consequence, all the results obtained from Eq. (25) with the various Fourier
303 coefficients A_m , (see Appendix A) give surprisingly the same exact results at node
304 abscissa, while initial shape of temperature distribution into the edge element
305 propagates to the others as shown in Fig. 4 *a*) and *b*).

306

307 In case of Heaviside distribution of temperature, due to the initial jump discontinuity at
308 boundaries, the discontinuities propagates between nodes with time evolution. A well-
309 known Gibbs phenomenon occurs at the transitions to/from the vertical sections, i.e. an
310 overshoot of the Fourier sums, limited to 18% of the jump value [39], that rapidly
311 converges toward the midpoint of the jump equal to the values of the horizontal
312 section, especially when the number of harmonics, m , used for numerical computation
313 increases. For instance, with computation of 10^6 harmonics, this phenomena is so
314 concentrated that it cannot appear on the presented plots in Fig. 4.

315

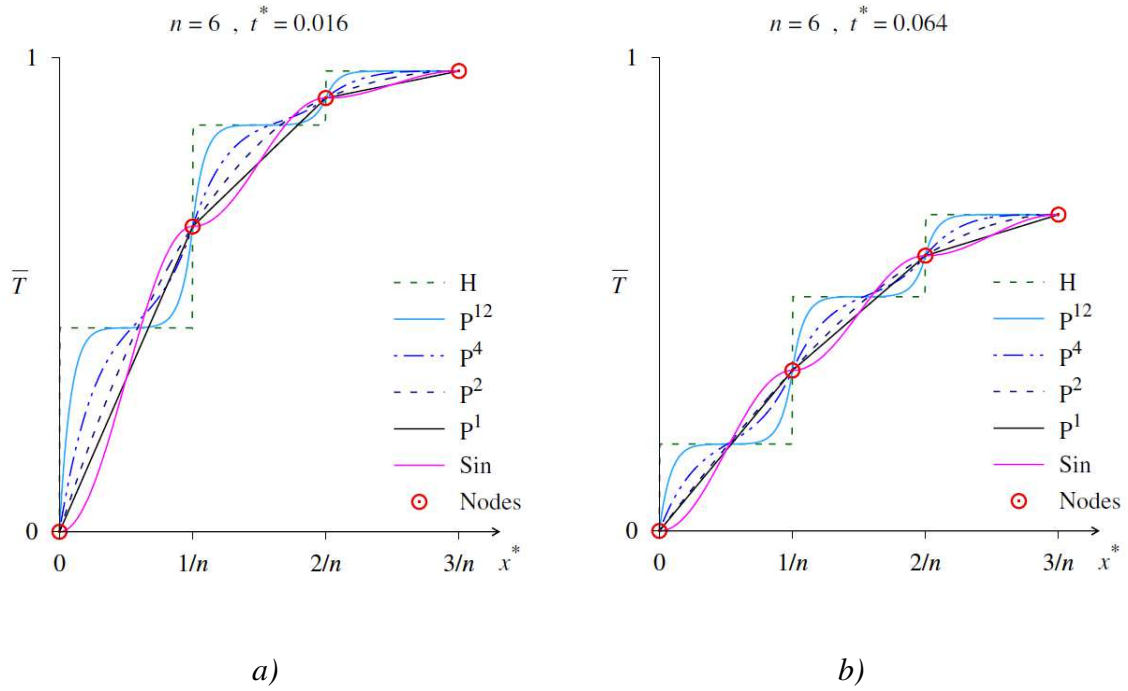


Fig. 4 : Extended exact temperatures of the discrete system in a half part of a 6 elements system at dimensionless time: – a) $t^* = 0.016$; – b) $t^* = 0.064$

316
317
318

319 In case of semi-infinite system, $L \rightarrow \infty$ and $t^* \rightarrow 0$ according to Eq. (7) while $n \rightarrow \infty$ as
320 well. This particular case cannot be directly compared with the considered discrete
321 system but with the continuous one.

322

323 Semi-infinite system with an imposed temperature at the border, T_0 , are classically
324 studied. As in the finite system, for an infinite elapsed time, temperatures tends
325 asymptotically towards T_0 , when $t \rightarrow \infty$, while the temperature decreases
326 instantaneously in the whole chain for $t > 0$. Since $n \rightarrow \infty$, the difference equation
327 given into Eq. (1) is the same as the differential equation of the continuous case. It
328 finds the well-known solution of local parabolic Fourier equation, based on error
329 function, $\text{erf}(x)$, in case of the semi-infinite continuous medium:

$$\bar{T}_{\infty}(x^*, t^*) = \text{erf}\left(\frac{x^*}{2\sqrt{t^*}}\right) \quad (26)$$

330

331 Thereafter, this solution is used to compare the results from local and nonlocal models
332 with the exact temperature at some node abscissas, see Fig. 7.

333 4. Comparison between the lattice and the nonlocal solution

334

335 4.1. Continualization procedure

336 Based on a Taylor expansion of the spatial difference operator in Eq. (8), the
337 continualization procedure considers that for a sufficiently smooth temperature
338 distribution of temperature $\bar{T}_i = \bar{T}(x = ia)$ and

$$\bar{T}(x+a, t) = \sum_{k=0}^{\infty} \frac{a^k \partial_x^k \bar{T}(x+a, t)}{k!} = e^{a\partial_x} \bar{T}(x, t) \quad (27)$$

339 where $\partial_x = \partial/\partial x$ is the spatial differentiation and $e^{a\partial_x}$ is a pseudo differential operator
340 as introduced for instance in [40] [41] and widely used for mechanical problems [42]
341 [43] [44] [45] [46].

342 By expanding the finite difference operator using Eq. (24), Eq. (8) can be
343 continualized as:

$$\bar{T}_{i+1} - 2\bar{T}_i + \bar{T}_{i-1} = (e^{a\partial_x} - 2 + e^{-a\partial_x}) \bar{T}(x, t) = 4 \sinh^2\left(\frac{a}{2} \partial_x\right) \bar{T}(x, t) \quad (28)$$

344 The pseudo-differential operator can be approximated by the following Taylor
345 expansion, if the considered hold sufficiently smooth variation:

$$\frac{4}{a^2} \sinh^2\left(\frac{a}{2} \partial_x\right) = \partial_x^2 + \frac{a^2}{12} \partial_x^4 + \mathcal{O}(a^4) \quad (29)$$

346 which leads to a gradient-type temperature diffusion problem with the square of
347 characteristic length, l_c^2 , equal to $a^2/12$ [2].

348 A numerical solution could be directly computed from the second-order continualized
349 equation, which may be expressed as a gradient heat equation with higher-order
350 temperature gradient terms. A similar methodology of expanding difference operators
351 for lattice diffusion processes has been used by Weymann (1967) [25], Taitel (1972)
352 [26] and more recently by Sobolev (1992, 2014) [27] [28]. Theses authors considered a
353 lattice ruled by a linear random walk equation (another kind of lattice), which is a
354 discrete system both in space and in time, as opposed to the thermal lattice considered
355 in this paper which is only discrete in space. The pseudodifferential operator can also
356 be efficiently approximated by Padé's approximant to avoid higher-order gradient
357 terms and additional difficulties related to higher-order boundary conditions. Such

358 rational expansion of the pseudodifferential operator has been successively applied to
 359 mechanical problems such as vibration of axial lattices [44] [45] [40] [41].

360

361 A numerical solution could be directly computed from the second-order continualized
 362 equation, however, the pseudo-differential operator can also be efficiently
 363 approximated by Padé's approximant to compute dynamic responses [44] [45] [40]
 364 [41], or recently in cases of of linear elastic lattice [47], even inelastic lattice such as
 365 damage mechanics [48] or elastoplastic problems [49].

366

367 To avoid the difficulties associated with higher-order boundary conditions needed in
 368 the resolution of such continualized schemes [50], Padé's approximation of the finite
 369 difference Laplacian is introduced:

$$\frac{4}{a^2} \sinh^2\left(\frac{a}{2} \partial_x\right) = \frac{\partial_x^2}{1 - \frac{a^2}{12} \partial_x^2} + \dots \quad (30)$$

370 to turn the Eq. (28) into analytical formulation:

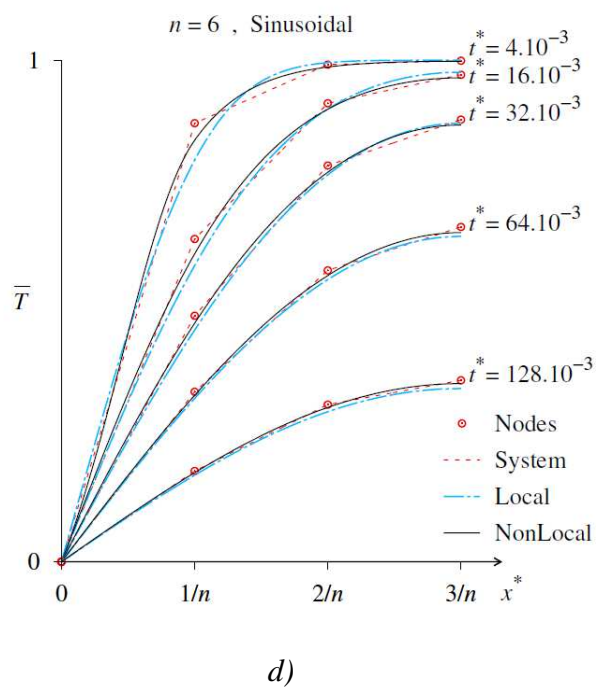
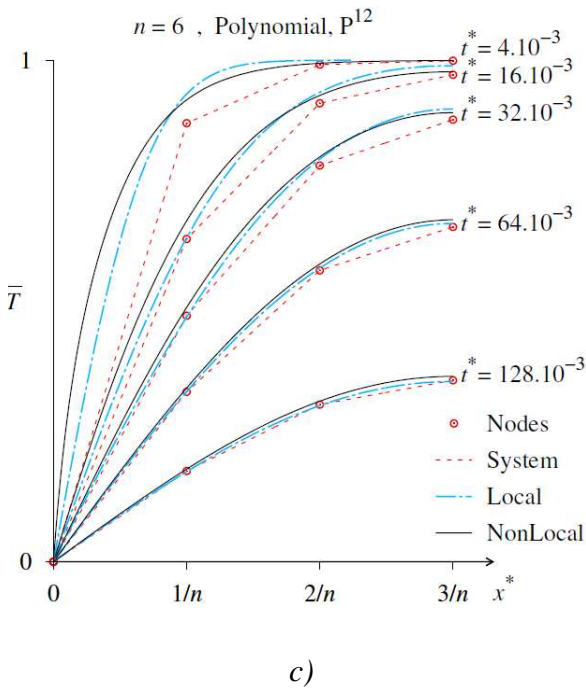
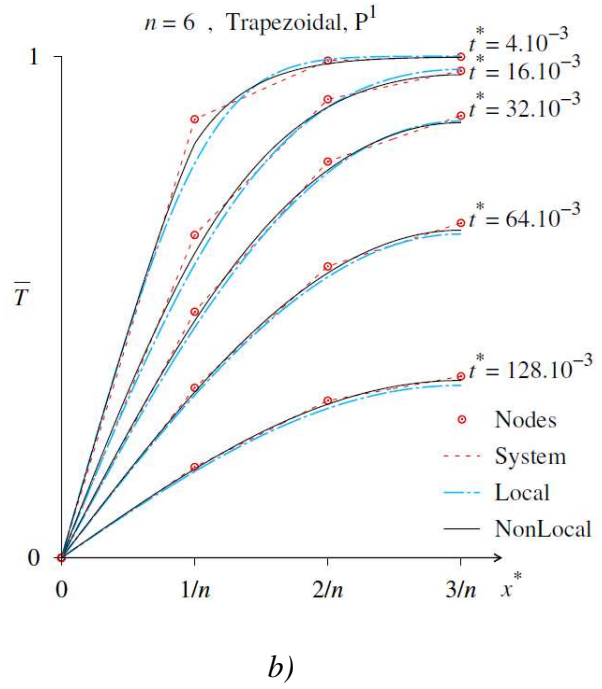
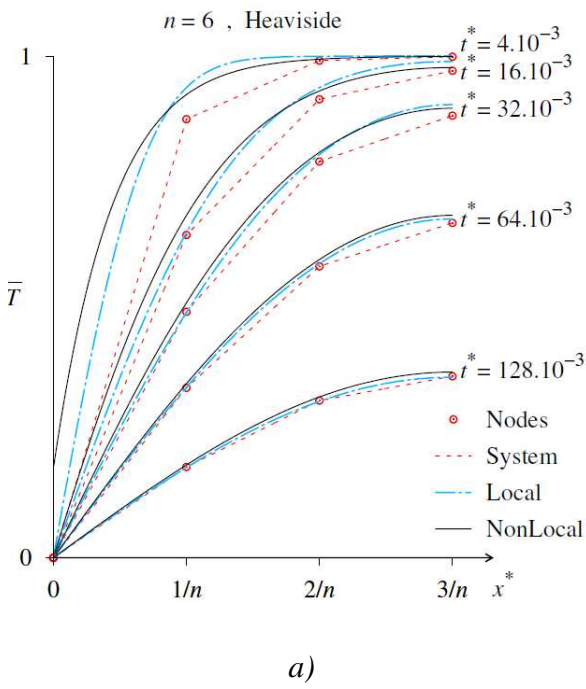
$$\bar{T}^{\&e} = \bar{T}'' + l_c^{*2} \bar{T}^{\&e} \quad \text{with} \quad l_c^{*2} = \frac{a^2}{12L^2} = \frac{1}{12n^2} \quad (31)$$

371 This nonlocal diffusion law is physically supported by the cell length, a , of the
 372 periodical lattice heat model.

373

374 With this length scale calibration, analytical results are checked with numerical ones
 375 (see Appendix B) and compared with the exact solutions at the node of the discrete
 376 system, used as references. With a limited number, n , of cell elements, the scale effect
 377 departing continuous and discrete system are magnified. All plotted results are
 378 hereafter obtained with $n=6$. Due to the symmetry of the problem, the first half part of
 379 the rod is only presented, allowing a better focus on the evolution of temperature
 380 distribution at the edge. Local and nonlocal heat profiles are plotted at various
 381 dimensionless time in Fig. 5.

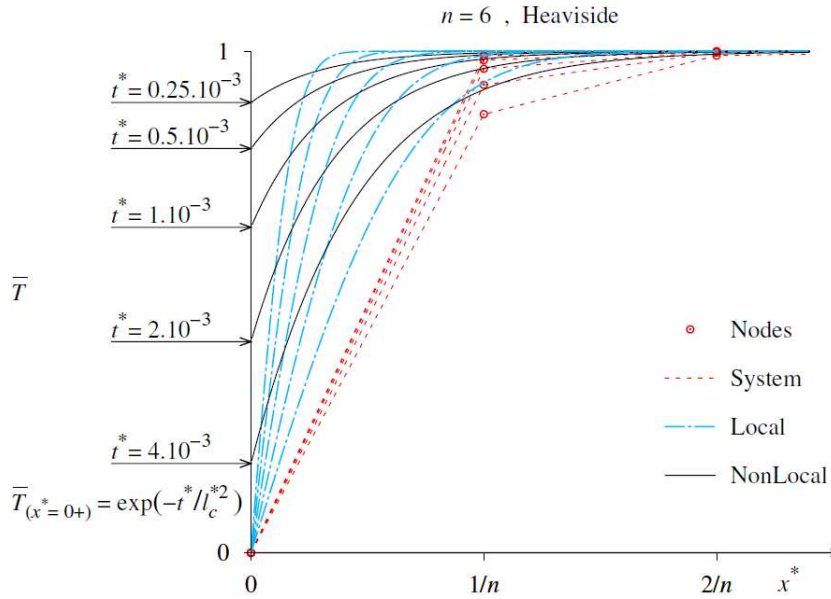
382



384 *Fig. 5 : Temperature profiles of the left half part of a $n=6$ elements system for some*
 385 *dimensionless times ranging from 4.10^{-3} to 128.10^{-3} with initial temperature*
 386 *distribution into the edge elements corresponding to:*
 387 *– a) Heaviside case; – b) Trapezoidal, P^1 ; – c) Polynomial P^{12} ; – d) Sinusoidal.*
 388

390 4.2. Boundary discontinuity in Heaviside case

391 As observed in Fig. 5 a), in case of Heaviside initial temperature distribution, the
 392 nonlocal model highlights an unexpected temperature discontinuity at the boundary for
 393 the shortest evolution times. A focus on this discontinuity phenomenon for shorter
 394 evolution time with the same $n = 6$ elements system is presented in Fig. 6.
 395



396
 397 *Fig. 6 : Focus on discontinuities of temperature at the boundaries of a $n=6$ elements*
 398 *system in case of Heaviside initial temperature distribution at beginning of evolution,*
 399 *for dimensionless times ranging from $0.125 \cdot 10^{-3}$ to $4 \cdot 10^{-3}$.*
 400

401 Barenblatt et. al [11] obtained a similar nonlocal diffusion equation as presented in
 402 Eq. (2). They demonstrate that first boundary value problem dealing with the theory of
 403 non-steady-state seepage in fissured rock induces a jump in state parameter due to the
 404 discontinuity of the initial conditions, at the rod extremities in Heaviside case.

405 Here, the difference between temperature $T(0+,t) - T(0-,t)$ and $T(L-,t) - T(L+,t)$,
 406 can be analytically identified on both sides of discontinuity, as shown by Barenblatt et.
 407 al [11]. A short demonstration is presented in Appendix C. Hence, the temperature
 408 evolution at the inside borders can be expressed a dimensionless form:

$$\bar{T}(0+, t^*) = \exp\left(-\frac{t^*}{l_c^2}\right) = \bar{T}(1-, t^*) \quad (32)$$

409 As a consequence, the initial discontinuity propagates with a decreasing range in time
410 according to Eq. (32). This relationship match perfectly the analytical results of the
411 nonlocal model calibrated with $l_c^2 = a^2/12$ or $l_c^{*2} = 1/12n^2$, plotted in Fig. 6.

412 4.3. Efficiency of the nonlocal diffusion model to predict the nodes temperature

413 The nonlocal model does not predict always the node temperature with a better
414 accuracy than the local one. As shown in Fig. 5, for a given node, the efficiency of the
415 nonlocal model depends on the node abscissa and evolution time. The difference
416 between the exact node temperature and predictions according to the local and
417 nonlocal models of a $n = 6$ elements system are plotted versus time evolution at the
418 first nodes beyond the boundary (i.e. $i = 1$ or $i = n - 1$) in Fig. 7 a) and c) at the mid
419 node (i.e. $i = n/2$) in Fig. 7 b) and d).

420

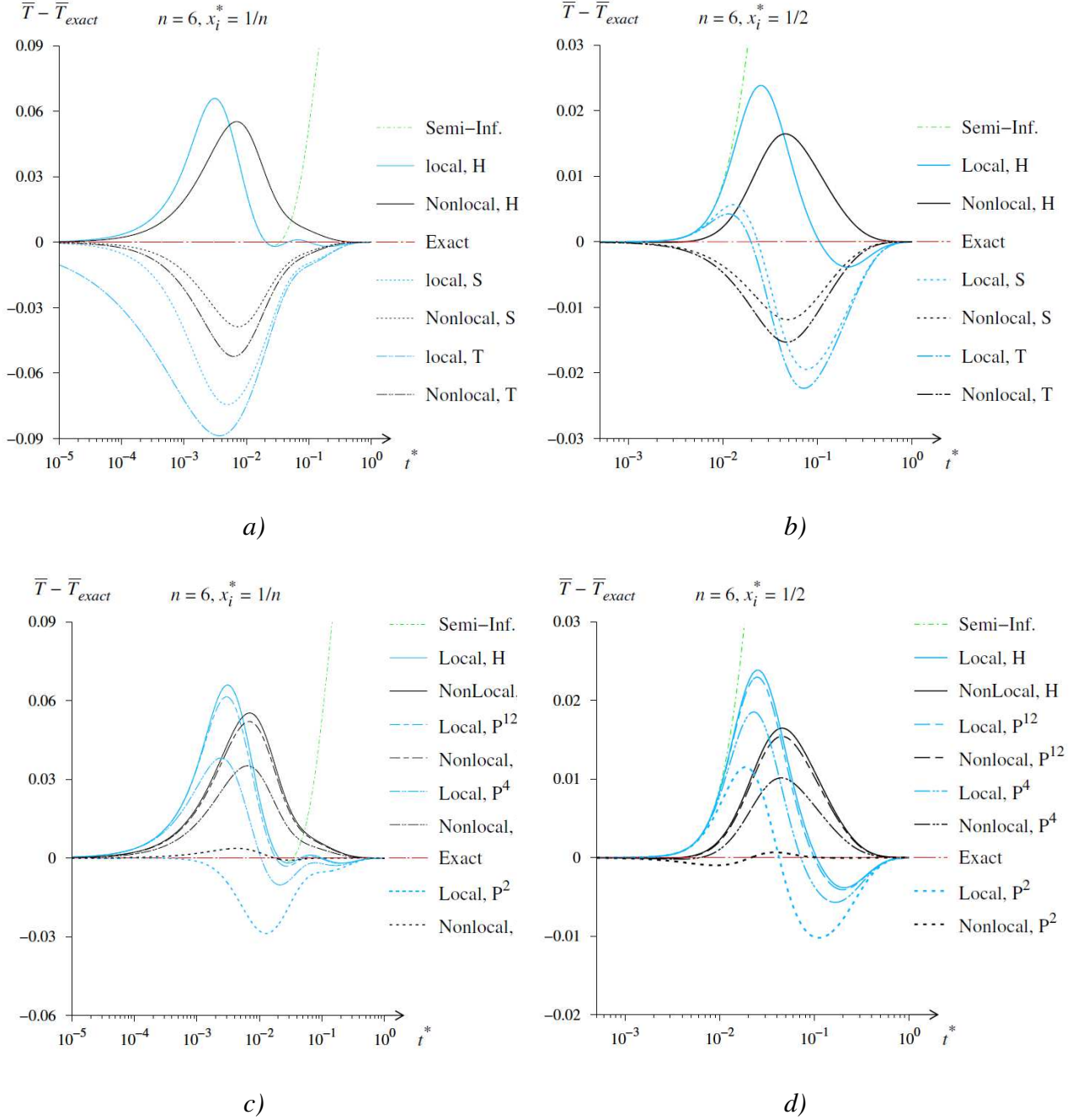
421 It can be checked that all models predict normalized temperature below than the semi-
422 infinite continuous system at the mid node, see Eq. (26). However, at the first node,
423 close to the imposed gap of temperature, only local models remain below the local
424 semi-infinite predictions, see Fig. 7 c). The exact temperature at the first node of 6-
425 elements system is actually slightly higher than the semi-infinite continuous system at
426 the same abscissa when t^* is close to 2.10^{-2} . In case of Heaviside boundary condition,
427 the nonlocal model integrates such size effect on temperature at the first node, as
428 shown in Fig. 5, but this increase in temperature is largely magnified, especially at
429 earlier evolution time.

430

431 As shown in Fig. 7, whatever the boundary condition, the magnitude of the difference
432 with the exact temperature is always higher with local models than with the nonlocal
433 ones, meaning a better accuracy of the enriched model based on nonlocal
434 considerations.

435 At the mid node as well as the first node, the Polynomial P^2 boundary condition leads
436 to the better fit of the exact values, while the Heaviside and the Trapezoidal conditions
437 lead to a less efficient prediction. As the Polynomial degree increases, the initial
438 temperature distribution tends toward the Heaviside one and the discrepancy of the
439 results increases. Finally, the Sinusoidal initial condition lead to similar but smaller
440 differences than those obtained with Trapezoidal condition, probably due to the

441 continuity of the spatial derivative of temperature included with the trigonometric
 442 continualization process.
 443

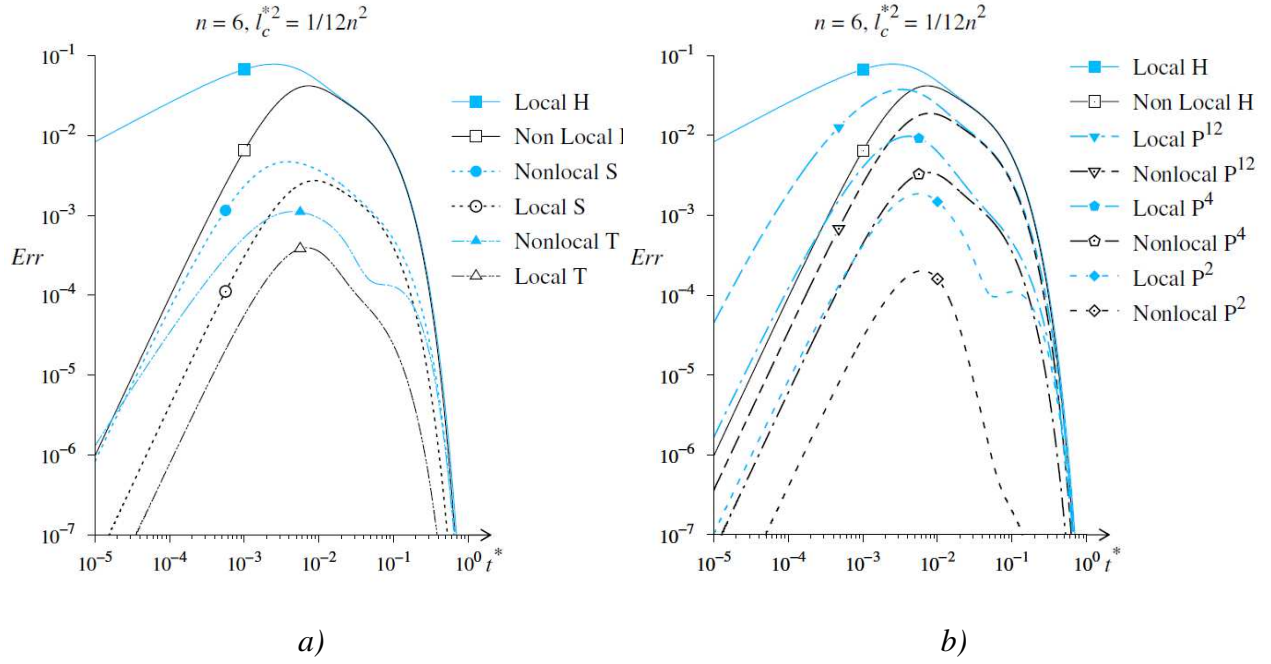


444 *Fig. 7 : Evolution of differences between normalized temperature of the models (local*
 445 *and nonlocal) and the exact ones for a $n = 6$ elements system:*
 446 *– c) at node 1 or $(n-1)$ with Heaviside, Trapezoidal and Sinusoidal boundary*
 447 *conditions*
 448 *– a) at the mid length (i.e. node $n/2$) with Heaviside, Trapezoidal and Sinusoidal*
 449 *boundary conditions*
 450 *– d) at node 1 or $(n-1)$ with Heaviside, Polynomial, P^2 , P^4 , and P^{12}*
 451 *– b) at the mid length (i.e. node $n/2$) with Heaviside, Polynomial, P^2 , P^4 , and P^{12}*

452
 453 The efficiency of the models according initial conditions depends on both node
 454 abscissa and time evolution. As the result of the comparison between local and
 455 nonlocal model for given condition and node could change drastically with time
 456 evolution, the efficiency of models is globally compared for all node temperatures
 457 introducing a time dependent error function, $Err(t^*)$, based on the residual sum of
 458 squares, i.e. $\sum (\bar{T}_i - \bar{T}_{i,exact})^2$. Both term of temperature are theoretically null at the
 459 edge nodes. The mean squared error at the other nodes can be computed from Eq. (25)
 460 and Eq. (24), through the Err function :

$$Err(t^*) = \frac{1}{n-1} \sum_{i=1}^{n-1} \sum_{m=1}^{\infty} \left[A_m \sin\left(\frac{m\pi i}{n}\right) \right]^2 \left[\exp\left(\frac{-m^2 \pi^2 t^*}{1+m^2 \pi^2 l_c^{*2}}\right) - \exp\left(-4n^2 \sin^2\left(\frac{m\pi}{2n}\right) t^*\right) \right]^2 \quad (33)$$

461
 462 It should be noted here, that edge node temperature is actually not null for Heaviside
 463 initial assumption, see Eq. (32). If the whole nodes are considered, The Err function of
 464 the nonlocal model in the Heaviside case would be higher in the first instants of the
 465 evolution.
 466 For small n values, the difference between nonlocal and local model is magnified, i.e.
 467 in presence of strong scale effect induced by the microstructure. Fig. 8 shows the
 468 global efficiency of the nonlocal model for a $n=6$ system. For a given initial
 469 temperature distribution, $Err(t^*)$ is always lower for the nonlocal model than for the
 470 local one. The Fig. 8 b) confirms that Polynomial P^2 initial temperature distribution
 471 associated with the considered nonlocal model gives the most efficient prediction,
 472 while the Heaviside condition lead the greater value of $Err(t^*)$. Moreover, the nonlocal
 473 and local model tends rapidly toward the same highest residual value, beyond $t^* = 10^{-2}$
 474 with Err function computed from the $n-1$ centered nodes. Whatever initial
 475 conditions, the nonlocal model gives significantly less residual values at nodes on the
 476 whole studied time evolution, i.e. with $10^{-5} < t^* < 1$.



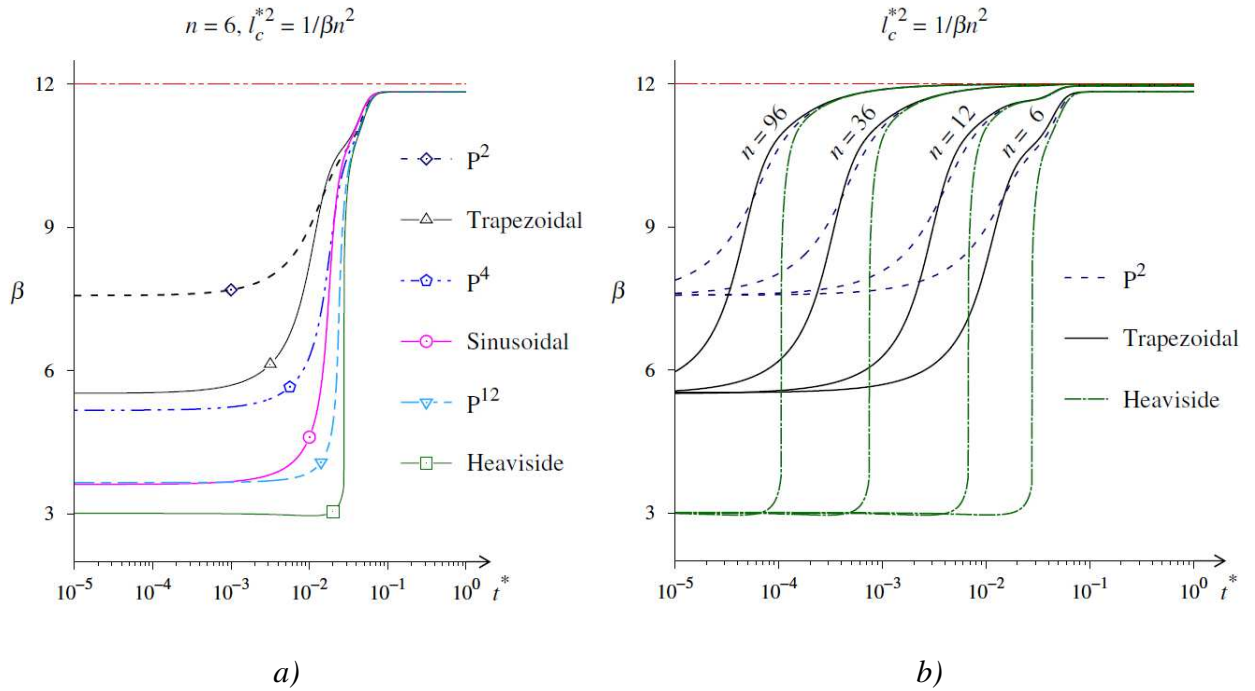
477 *Fig. 8 : Time evolution of the residual sum of squares at node abscissa of the models*
 478 *(local and nonlocal), Err, for a $n = 6$ elements system:*
 479 *– a) with Heaviside, Trapezoidal and Sinusoidal boundary conditions*
 480 *– b) with Heaviside, Polynomial, P^2 , P^4 , and P^{12} .*
 481

482 4.4. Length scale calibration

483 In order to calibrate the length scale, the optimal characteristic length $l_{c,opt}^2$, associated
 484 to the nonlocal model is introduced. The Eq. (31) can be written according a second
 485 variable, β , such as $l_{c,opt}^2 = a^2/\beta$, equivalent to $l_{c,opt}^{*2} = 1/\beta n^2$. The minimum of
 486 $Err(t^*, \beta)$ provides the β value, i.e. the optimal characteristic length $l_{c,opt}^2$. The value
 487 of β can be computed according t^* by solving $\partial Err/\partial \beta = 0$, that can be numerically
 488 computed as follow :

$$(n-1) \frac{\partial Err}{\partial \beta}(t^*, \beta) = \sum_{i=1}^{n-1} \sum_{m=1}^{\infty} \left[A_m \sin\left(\frac{m\pi i}{n}\right) \right]^2 \left\{ \begin{array}{l} 2t^* \left(\frac{n}{\beta(n/m\pi)^2 + 1} \right)^2 \exp\left(\frac{-\beta n^2 t^*}{\beta(n/m\pi)^2 + 1}\right) \\ \left[\exp\left(-4n^2 \sin^2\left(\frac{m\pi}{2n}\right)t^*\right) - \exp\left(\frac{-\beta n^2 t^*}{\beta(n/m\pi)^2 + 1}\right) \right] \end{array} \right\} = 0 \quad (34)$$

489 $\partial Err/\partial \beta$ is a monotonic increasing function of β , and the numerical resolution of
490 Eq. (34) gives only one solution, straightly assessed through numerical resolution. Fig.
491 9 shows that β tends rapidly toward 12, i.e. $l_{c,opt} \rightarrow l_c$, especially beyond $t^* = 10^{-2}$ for a
492 $n = 6$ elements system, and before this dimensionless time when n increases. The
493 asymptotic value of β for higher values of t^* is also closest to 12 when n increases. As
494 already observed with such nonlocal diffusion law [2], the time independent length
495 scale, $l_c^2 = a^2/12$, is reached after a transitory time, inversely proportional to the
496 number of lattice element, n , see Fig. 9 b).
497 In accordance with the previous observations about the prediction accuracy according
498 to initial temperature distributions, the Polynomial P² and Trapezoidal conditions give
499 the closest values of l_c^2 at the beginning of evolution, while the Heaviside one gives
500 the farthest.



501
502
503
504

Fig. 9 : Numerical evaluation of $\beta = (n^2 l_{c,opt}^{*2})^{-1}$
– a) as a function of time (t^*) with the considered initial conditions
– b) as a function of time (t^*) according to various values of n

505 4.5. Prediction of heat flow at boundaries

506 The outlet heat flow density at boundaries in a dimensionless and normalized form is
 507 introduced: $\bar{\varphi}_0$, at $x^* = 0$ or $\bar{\varphi}_1$, at $x^* = 1$. Eq. (3) and Eq. (7) lead to:

508 $\bar{\varphi}_0 = -\bar{\varphi}_{(x^*=0)} = \int_0^{1/2} \bar{T} dx^*$ or $\bar{\varphi}_{(x^*=1)} = -\int_{1/2}^1 \bar{T} dx^*$. Due to symmetrical conditions it can be
 509 easily checked that $\bar{\varphi}_0 = \bar{\varphi}_1$.

510 Time derivation and space integration of Eq. (24) give the solution of $\bar{\varphi}_0$ for both local
 511 ($l_c^* = 0$) and nonlocal models as follow:

$$\bar{\varphi}_0 = \pi \sum_{m=1}^{\infty} \frac{mA_m}{1+m^2\pi^2l_c^{*2}} \exp\left(\frac{-m^2\pi^2t^*}{1+m^2\pi^2l_c^{*2}}\right) \quad (35)$$

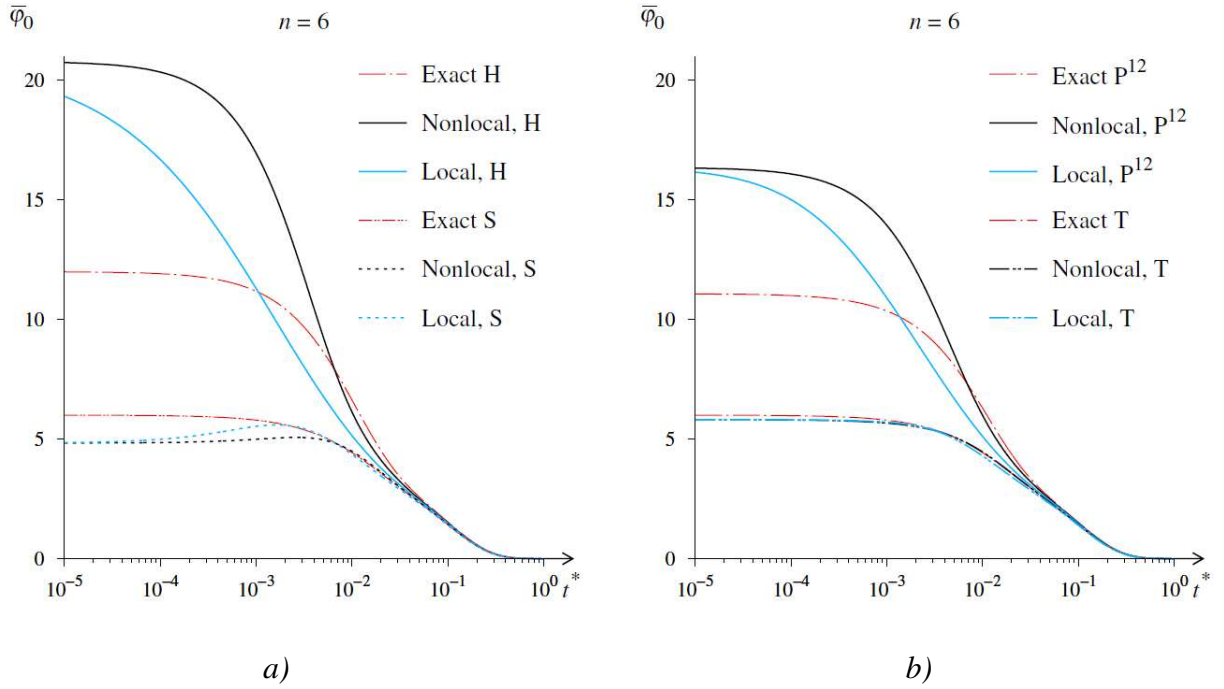
512 where A_m is the series coefficient defined according to the initial conditions, see
 513 Eq. (18), and Appendix A.

514 In a same way, the exact solution $\varphi_{0,exact}^*$ used as a reference is obtained by time
 515 derivation and space integration of Eq. (13).

$$\bar{\varphi}_{0,exact} = \frac{4n^2}{\pi} \sum_{m=1}^{\infty} \frac{A_m}{m} \sin^2\left(\frac{m\pi}{2n}\right) \exp\left[-4n^2 \sin^2\left(\frac{m\pi}{2n}\right)t^*\right] \quad (36)$$

516 Only derivation of the time dependent departs from models. Time evolution of φ_0^* for
 517 the initial conditions giving the greater differences are plotted in Fig. 10 a) and b).

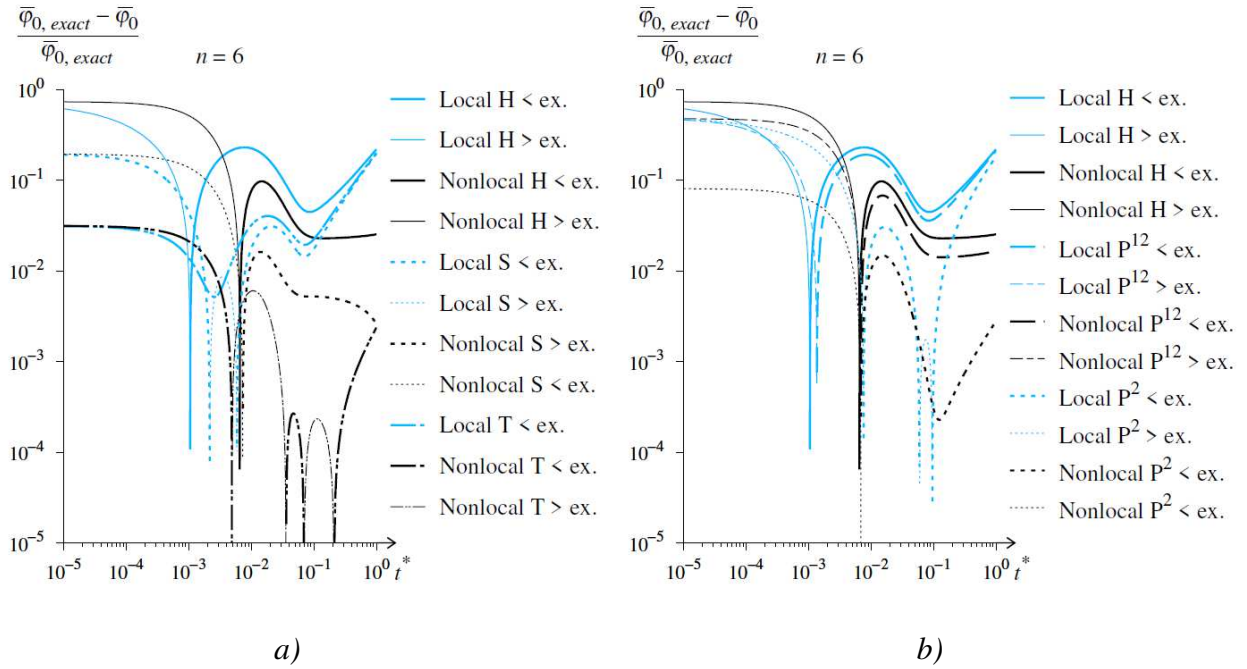
518



520 *Fig. 10 : Time evolution of the normalized outgoing heat flow density at boundaries,*
 521 *– a) for Heaviside and Sinusoidal initial conditions*
 522 *– b) for Polynomial P^{12} and Trapezoidal initial conditions*
 523

524 $\bar{\varphi}_{0,exact}(t^*)$ is the same for Sinusoidal and Trapezoidal cases. This means that for a
 525 same initial continuous amount of heat, $\bar{\varphi}_{0,exact}(t^*)$ does not depend on its initial
 526 distribution. The increasing degree of polynomial initial temperature distribution
 527 induces a continuous evolution from trapezoidal (P^1) toward Heaviside (to P^{12}). To
 528 analyze the efficiency of the models about outgoing heat flow density, the relative
 529 differences $(\bar{\varphi}_{0,exact} - \bar{\varphi}_0) / \bar{\varphi}_{0,exact}$ are plotted in Fig. 11.

530



531 *Fig. 11 : Relative difference between the exact, $\bar{\varphi}_{0,exact}$, and local and nonlocal*
532 *outgoing heat flow density at boundaries, $\bar{\varphi}_0$, versus dimensionless time evolution t^* .*
533 *– a) for Heaviside, Sinusoidal and Trapezoidal initial conditions*
534 *– b) for Heaviside and Polynomial P^{12} , P^4 and P^2 initial conditions*
535

536 Along the studied evolution time, numerous curves intersections occur from same
537 initial condition, and analysis may not be trivial. However, the main global tendencies
538 are :

539 – At the earliest time of evolution the nonlocal as the local model largely overestimate
540 the values $\bar{\varphi}_0$ in comparison of $\bar{\varphi}_{0,exact}$ and nonlocal model is far to be efficient until
541 $t^* = 8.10^{-3}$ in the case of $n = 6$ elements system.

542 – After a transitory step, the superiority of the nonlocal model as compared to the local
543 model appears. Depending on the number n of element, this step occurs approximately
544 when $t^* = 8.10^{-3}$ for $n = 6$ i.e. when the decrease in mid node normalized temperature
545 reaches 0.5%. If the value of n increases, this step occurs earlier as the beginning of
546 the convergence time of β toward 12 does, see Fig. 9 b). Beyond this transitory time,
547 the nonlocal model gives better results than the local one, except for Polynomial P^2
548 initial case where the local model could be still punctually better.

549

550 4.6. Prediction of the global amount of heat

551 The amount of heat Q (in joule), or for instance the internal energy of the rod with a
 552 cross section area equal to S , can be deduced from:

$$Q(t) = \rho CS \int_0^L T(x,t) dx \text{ equivalent to} \quad (37)$$

$$\bar{Q}(t^*) = \int_0^1 \bar{T}(x^*, t^*) dx^* = \bar{Q}(0) - 2 \int_0^{t^*} \phi_0^* dt^* \text{ with } \bar{Q} = \frac{Q}{\rho S L C \Delta T} - \frac{T_0}{\Delta T}$$

553 where $\bar{Q}(t^*)$ is the normalized amount of heat equal to the average temperature along
 554 the finite continualized rod. Based on Eq. (24) or on Eq. (35), $\bar{Q}(t^*)$ from local ($l_c^*=0$)
 555 and nonlocal models, according to the considered system, is computed as follow:

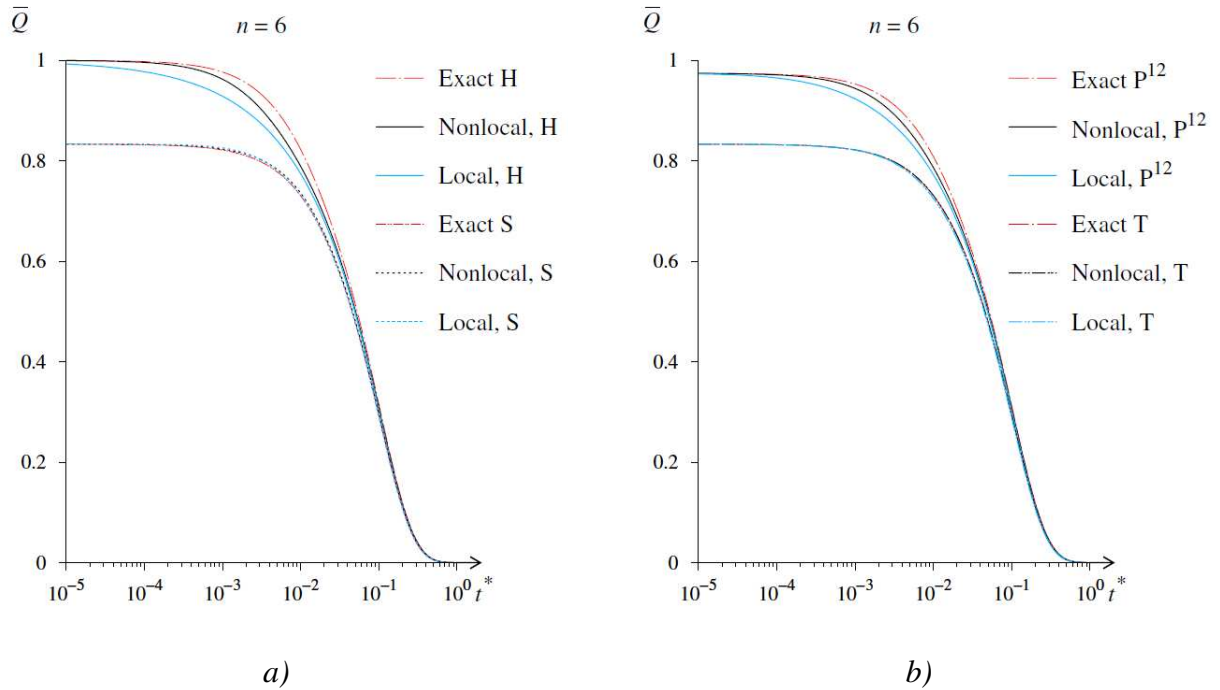
$$\bar{Q}(t^*) = \frac{2}{\pi} \sum_{m=1}^{\infty} \frac{A_m}{m} \exp\left(\frac{-m^2 \pi^2 t^*}{1 + m^2 \pi^2 l_c^{*2}}\right) \quad (38)$$

556 The same spatial dependent term is found in Eq. (24) and Eq. (25) defining
 557 $\bar{T}_{exact}(x_i^*, t^*)$. Only the time dependent term departs and integration of \bar{T}_{exact} gives the
 558 mean values of the exact temperature over the whole continualized system as stated in
 559 Eq. (37). The exact solution $\bar{Q}(t^*)_{exact}$ used as reference is then computed for each
 560 initial temperature distribution from Eq. (25) as:

$$\bar{Q}(t^*)_{exact} = \frac{2}{\pi} \sum_{m=1}^{\infty} \frac{A_m}{m} \exp\left[-4n^2 \sin^2\left(\frac{m\pi}{2n}\right) t^*\right] \quad (39)$$

561 It should be noted that according to the initial distribution $\bar{T}(x^*, 0)$ defined in section
 562 2.2, $\bar{Q}(t^*=0) = 1$ in Heaviside case, $\bar{Q}(t^*=0) = 1 - 2/n(p+1)$ in Polynomial case with a
 563 degree equal to p , and $\bar{Q}(t^*=0) = 1 - 1/n$ in Trapezoidal and Sinusoidal cases, see Fig. 12
 564 with $n=6$. Moreover, as shown in section 2.2, the exact temperature at the node
 565 $\bar{T}_{i,exact}(t^*)$ does not depend on initial distribution of temperature since all the Fourier
 566 series coefficients used in Eq. (25) produce the same results at nodes. The shape of the
 567 initial temperature distribution into the edge element propagates into all elements
 568 during evolution, see Fig. 4 and integration of Eq. (25) over the whole length removes
 569 the space dependent term. As a consequence, the ratio $\bar{Q}_{exact}(t^*)/\bar{Q}_{exact}(t^*=0)$ remains
 570 the same whatever the initial condition considered (i.e. whatever the selected A_m

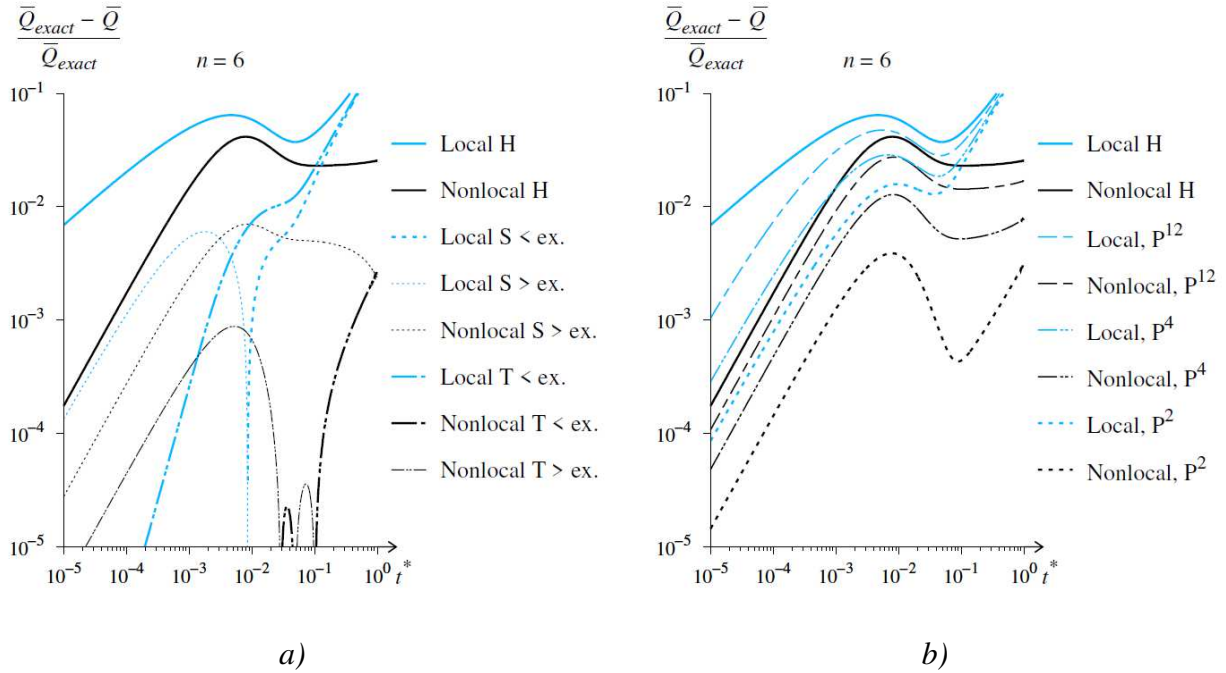
571 coefficient). For instance, $\bar{Q}_{exact}(t^*)$ is the same for Sinusoidal and Trapezoidal case,
 572 as it can be already observed with $\bar{\varphi}_0$ in Fig. 11.
 573



574 *Fig. 12 : Time evolution of the normalized amount of heat into the system*
 575 *– a) for Heaviside and Sinusoidal initial conditions*
 576 *– b) for Polynomial P^{12} and Trapezoidal initial conditions*
 577

578 Evolution of \bar{Q} , plotted in Fig. 12, shows that both local and nonlocal models
 579 underestimate the remaining amount of heat into the system during the evolution in
 580 Heaviside and similar boundary condition as polynomial P^{12} while the curves are very
 581 closed without clear tendency in sinusoidal or Trapezoidal case. The differences with
 582 the exact case are detailed in Fig. 13 for each initial case.
 583

584 Results show that the nonlocal model give better prediction than the local one, from
 585 the beginning of the evolution, to predict the amount of heat, in particular with
 586 Heaviside and Polynomial, Trapezoidal included, initial conditions, see Fig. 13 b). In
 587 these cases, local model leads to a significant underestimation in comparison of the
 588 nonlocal model, especially at the beginning of the evolution, until $t^* = 8 \cdot 10^{-3}$ with
 589 $n = 6$, when the scale effect results in a delayed diffusion.
 590



591 *Fig. 13 : Relative difference between amount of heat deduced from exact formulation*
 592 *\bar{Q}_{exact} and from local and nonlocal model \bar{Q} versus dimensionless time evolution t^* .*
 593 *– a) for Heaviside, Sinusoidal and Trapezoidal initial conditions*
 594 *– b) for Heaviside and Polynomial P^{12} , P^4 and P^2 initial conditions*
 595

596 For Trapezoidal as for sinusoidal initial condition, the curves intersect at many times
 597 the exact results, see Fig. 13 a). Except for lower values of t^* , in case of trapezoidal
 598 initial conditions, the nonlocal model is significantly better, very closed to the exact
 599 solution, \bar{Q}_{exact} , with alternation of slight over and underestimation of the amount of
 600 heat, compared to the exact solution.

601 Globally, beyond a transitory time, for instance after $t^* = 8.10^{-3}$ with $n = 6$ elements.
 602 the nonlocal model gives a better prediction of the remaining total of heat amount \bar{Q}
 603 in comparison of the local one, whatever the initial temperature distribution into the
 604 edges elements. This transitory step becomes shorter when n tends to be larger.
 605 Increasing value of n induces a lower relative error of the models but tends to magnify
 606 the relatives differences induced by the initial condition.

607

608 **5. Conclusion**

609 Thermal diffusion in a one-dimensional periodically microstructured lattice can be
610 described within a quasi-continuum approach governed by a nonlocal Fourier's law,
611 similar to the differential model of Eringen [10] initially devoted to material elasticity.
612 This nonlocal Fourier law can be also cast into a more general Guyer-Krumhansl type
613 model [5].

614
615 Using a continualization procedure, the characteristic length scale of the nonlocal heat
616 model is calibrated from the lattice spacing, a . This calibration appears also to be
617 optimal, since minimization of the sum of squares of residuals node temperature makes
618 the square of this length scale, with time evolution and/or increasing number of
619 element n , rapidly converge toward $l_c^2 = a^2/12$.

620
621 Despite strong discontinuity of the initial temperature profile, like in the case of
622 uniform initial temperature introduced from Heaviside operator, the continualized
623 nonlocal heat model based on a Padé asymptotic expansion of the spatial difference
624 operator (of the associated lattice problem) is able to capture scale effect. The nonlocal
625 model produces a better global prediction of the node temperatures than local model
626 (without any length scale), as compared to the exact thermal lattice solution. The
627 nonlocal model also predicts more efficiently the remaining amount of heat into the
628 discrete systems.

629
630 It is shown that the efficiency of the continualized nonlocal model to predict the
631 accurate temperature field of the lattice problem is sensitive to the continualized initial
632 conditions, especially at the border of the microstructured rod. A difficult question
633 consists in extending the discrete nodal temperature outside the lattice nodes, for the
634 computation of the continualized nonlocal problem. The continualized nonlocal model
635 gives better results for smoothed continualized initial conditions, in particular for a
636 parabolic temperature distribution (named here as P^2) into the edge elements.
637 However, the sinusoidal initial condition does not make the nonlocal model produce
638 better results than the trapezoidal condition. The presented nonlocal model, initially
639 based on sufficiently smooth variation of temperature is not affected by the initial
640 gradient continuity, while it is able to remain relevant for temperature discontinuity in

641 case of imposed jump at boundaries. But in this last case, the asymptotic solution at the
642 inner boundary differs from the imposed value at the extremities.

643

644 The present spatially nonlocal model, is able to predict delayed diffusion phenomena
645 in thermal lattices ruled by mixed differential-difference equations. It is probably
646 possible to extend such nonlocal model for discrete problems with both space and time
647 discreteness, leading to generalized nonlocal continuous diffusion problems, both in
648 space and in time.

649

650 **Declaration of competing interest**

651 The authors declare that they have no known competing financial interests or personal
652 relationships that could have appeared to influence the work reported in this paper.

653

654 **Acknowledgement**

655 The authors thank Dr. Yassine Belmoujahid for fruitful discussions on numerical
656 simulation of thermal lattices.

657

659 **Nomenclature**

| | <i>Parameters</i> | <i>Dimension</i> | <i>Relative dimensionless parameters</i> |
|------------|--|--|--|
| a | Element length | [L] | $a^* = a/L = 1/n$ |
| $A_{k,m}$ | Fourier coefficients | – | |
| C | Specific heat capacity | $[L^2 \cdot T^{-2} \cdot \theta^{-1}]$ | |
| k | Harmonic of discrete Fourier summation | – | |
| l_c | Characteristic length of the Nonlocal model | [L] | $l_c^* = l_c/L$ |
| L | Length of the beam | [L] | |
| m | Harmonic of continuous Fourier series | – | |
| n | Number of elements | – | |
| p | Degree of the polynomial function | – | |
| Q | Amount of heat | $[M \cdot L^2 \cdot T^{-2}]$ | $\bar{Q} = Q / (\rho S L C \Delta T) - T_0 / \Delta T$ |
| S | Rod section | $[L^2]$ | |
| t | Elapsed time from initial state | [T] | $t^* = \alpha t / L^2$ |
| T | Temperature | [θ] | $\bar{T} = (T_0 - T) / \Delta T$ |
| x | Longitudinal coordinate | [L] | $x^* = x/L$ |
| α | Thermal diffusivity: $\alpha = \kappa / \rho C$ | $[L^2 \cdot T^{-1}]$ | |
| β | Variable associated to the optimal characteristic length $l_{c,opt}^2$ | – | $\beta = a^2 / l_{c,opt}^2$ |
| γ | Eigenvalue for time differential operators | – | |
| δ | Element partition for implicit finite difference computation | – | |
| λ | Eigenvalues for space differential operators | – | |
| ΔT | Imposed maximum gap of temperature at time $t = 0$ | [θ] | |
| κ | Thermal conductivity | $[M \cdot L \cdot T^{-3} \cdot \theta^{-1}]$ | |
| ξ | Space-temperature eigenfunction | – | |
| τ | Time-temperature eigenfunction | – | |
| ρ | Rod density | $[M \cdot L^{-3}]$ | |
| φ | Heat flux density | $[M \cdot T^{-3}]$ | $\bar{\varphi} = L\varphi / (\kappa \Delta T)$ |

661

662 **Appendix A: Fourier series**

663 Fourier summation coefficients for discrete system

664 The resolution at the node of the discrete system only needs finite Fourier series using
665 coefficients $A_k = (2/n) \sum_{p=1}^{n-1} \sin(k\pi p/n)$ that can be expressed as a single analytical
666 expression:

$$A_k = \sum_{p=1}^{n-1} \sin\left(k\pi \frac{p}{n}\right) = \text{Im} \left(\sum_{k=1}^{n-1} e^{jk\pi \frac{p}{n}} \right) = \text{Im} \left(\frac{e^{jk\pi \frac{n}{n}} - e^{jk\pi}}{1 - e^{jk\pi/n}} \right) = \frac{\sin^2\left(\frac{k\pi}{2}\right)}{\tan\left(\frac{k\pi}{2n}\right)} = \frac{1 - (-1)^k}{2 \tan\left(\frac{k\pi}{2n}\right)} \quad (40)$$

667

668 This relation allows to reduce computation of exact node solution to the single finite
669 summation of odd values of k given into Eq. (15).

670 Fourier series coefficients for continualized system

671 To satisfy the initial state solution of the continuous one-dimensional media,
672 continuous functions $\bar{T}_{ini}(x^*) = \bar{T}(x^*, 0)$ are defined for $x^* \in [0;1]$. The Fourier series
673 coefficient, A_m , are then defined as:

$$A_m = 2 \left[\begin{array}{l} \int_{(n-1)/n}^1 f_{edge}(1-x^*) \sin(m\pi x^*) dx^* \\ + \int_{1/n}^{(n-1)/n} \sin(m\pi x^*) dx^* \\ + \int_0^{1/n} f_{edge}(x^*) \sin(m\pi x^*) dx^* \end{array} \right] \quad (41)$$

674

675 Where $f_{edge}(x^*)$ is the initial distribution of temperature into the edge element,
676 defining the whole initial distribution of temperature $\bar{T}(x^*, 0)$ in the rod, see Eq. (17).

677 In order to verify $\bar{T}(x^*, 0) = \sum_{m=1}^{\infty} A_m \sin(m\pi x^*)$ according to Eq. (13) or Eq. (24), the

678 Fourier series coefficients with the various $f_{edge}(x^*)$ introduced into section 2.2 give :

679 – with an Heaviside initial distribution of temperature $\bar{T}(x^*, 0)$;

$$A_m^H = \frac{2}{m\pi} [1 - (-1)^m] \quad (42)$$

680

681 – with a “Trapezoidal” $\bar{T}(x^*, 0)$, or polynomial with $p = 1$, see Eq. (18);

$$A_m^{P1} = \frac{2n}{(m\pi)^2} [1 - (-1)^m] \sin\left(\frac{m\pi}{n}\right) \quad (43)$$

682

683 – with a “Polynomial” $\bar{T}(x^*, 0)$, with $p = 2$, see Eq. (18);

$$A_m^{P2} = \frac{2}{m\pi} [1 - (-1)^m] \left[1 - \cos\frac{m\pi}{n}\right] \quad (44)$$

684

685 – with a “Polynomial” $\bar{T}(x^*, 0)$, with an even value degree $p = 2q$ (where q is a
686 positive integer greater than 1), see Eq. (18);

$$A_m^{P2q} = \frac{2[1 - (-1)^m]}{m\pi} \left\{ \begin{array}{l} (-1)^{q+1} (2q)! \left(\frac{n}{m\pi}\right)^{2q} \left[1 - \cos\left(\frac{m\pi}{n}\right)\right] \\ + \sum_{j=1}^{q-1} \frac{(-1)^{(j+1)} (2q)!}{(2(q-j))!} \left(\frac{n}{m\pi}\right)^{2j} \end{array} \right\} \quad (45)$$

687

688 – with a “Sinusoidal” $\bar{T}(x^*, 0)$, see Eq. (19);

$$A_m^S = \frac{[1 - (-1)^m]}{m\pi} \left(\frac{n^2}{n^2 - m^2}\right) \left(1 + \cos\frac{\pi m}{n}\right) \quad (46)$$

689

690 In case of an infinite number of elements into the chain of length L , the initial
691 trapezoidal distribution of temperature become steeper and tends toward an Heaviside
692 function, i.e., toward an uniform one along the whole chain. Hence, when $n \rightarrow \infty$, it
693 can be checked that the Fourier series coefficients tends toward A_m^H .

694 It should be noted that due to initial conditions, all Fourier coefficients are null for
695 even values of m .

696

697 **Appendix B: Numerical resolution**

698

699 Semi-implicit finite difference method is applied to compute numerically the evolution
700 of temperature along the chain discretized according to $n\delta$ elements, with δ the
701 additional partition of each element giving the length discretization $\Delta x = L/n\delta$.
702 Presented computations, done to checked theoretical solutions, are made with $\delta = 500$.
703 To observe the large part of the diffusion process and be accurate at the beginning of
704 the heat diffusion. With $300 \times n$ computation times, time steps Δt^* are logarithmically
705 spaced into a range from 10^{-5} to 1, in order to get more accuracy at the beginning of
706 the evolution.

707

708 Symmetrical boundary conditions allows to compute only a half rod with $n\delta/2+1$ nodes
709 to optimize the solving process, leading to the following specific boundary conditions:

710 $\bar{T}_0^j = 0$ and adiabatic wall in the middle corresponding to $\bar{T}_{n\delta/2-1}^j = \bar{T}_{n\delta/2+1}^j$ while the
711 initial condition leads to $\bar{T}_1^0 = 0$ and $\bar{T}_i^0 = 1$ for $i > 1$ in the Heaviside case, or
712 $\bar{T}_i^0 = f_{edge}(\delta)$ for $i \leq p$ and $\bar{T}_i^0 = 1$ for $i > p$ in all other cases.

713

714 The dimensionless discrete local diffusion in Eq. (8) matches exactly the finite-
715 difference formulation. The continuous local heat equation can be numerically
716 computed according a Crank-Nicolson scheme, combining the stability of an implicit
717 method with the accuracy of a second order method in both space and time:

$$\frac{1}{\Delta t^*} (\bar{T}_i^{j+1} - \bar{T}_i^j) = \frac{1}{2(\Delta x^*)^2} (\bar{T}_{i+1}^{j+1} - 2\bar{T}_i^{j+1} + \bar{T}_{i-1}^{j+1} + \bar{T}_{i+1}^j - 2\bar{T}_i^j + \bar{T}_{i-1}^j) \quad (47)$$

718

719 Here both the left- and right-hand sides are centered at time step $j+1/2$, so the method
720 is second-order accurate in time, while a fully implicit method is only first-order
721 accurate in time [51].

722 The following system of $n\delta/2$ dimensionless equations allow to solve the node
723 temperatures of next time step \bar{T}_i^{j+1} according to the boundary conditions mentioned
724 above:

$$\begin{aligned}
& -\frac{(n\delta)^2}{2}\bar{T}_{i-1}^{j+1} + \left(\frac{1}{\Delta t^*} + (n\delta)^2\right)\bar{T}_i^{j+1} - \frac{(n\delta)^2}{2}\bar{T}_{i+1}^{j+1} = \\
& \frac{(n\delta)^2}{2}\bar{T}_{i-1}^j + \left(\frac{1}{\Delta t^*} - (n\delta)^2\right)\bar{T}_i^{j+1} + \frac{(n\delta)^2}{2}\bar{T}_{i+1}^{j+1}
\end{aligned} \tag{48}$$

725

726 The dimensionless discrete nonlocal diffusion equation, see Eq. (8) is reformulated
727 according to the same Crank-Nicolson finite difference scheme as:

$$\begin{aligned}
& \frac{1}{\Delta t^*}(\bar{T}_i^{j+1} - \bar{T}_i^j) = \frac{1}{2(\Delta x^*)^2}(\bar{T}_{i+1}^{j+1} - 2\bar{T}_i^{j+1} + \bar{T}_{i-1}^{j+1} + \bar{T}_{i+1}^j - 2\bar{T}_i^j + \bar{T}_{i-1}^j) \\
& + \frac{l_c^{*2}}{\Delta t^* \Delta x^{*2}}(\bar{T}_{i+1}^{j+1} - 2\bar{T}_i^{j+1} + \bar{T}_{i-1}^{j+1} - \bar{T}_{i+1}^j + 2\bar{T}_i^j - \bar{T}_{i-1}^j)
\end{aligned} \tag{49}$$

728

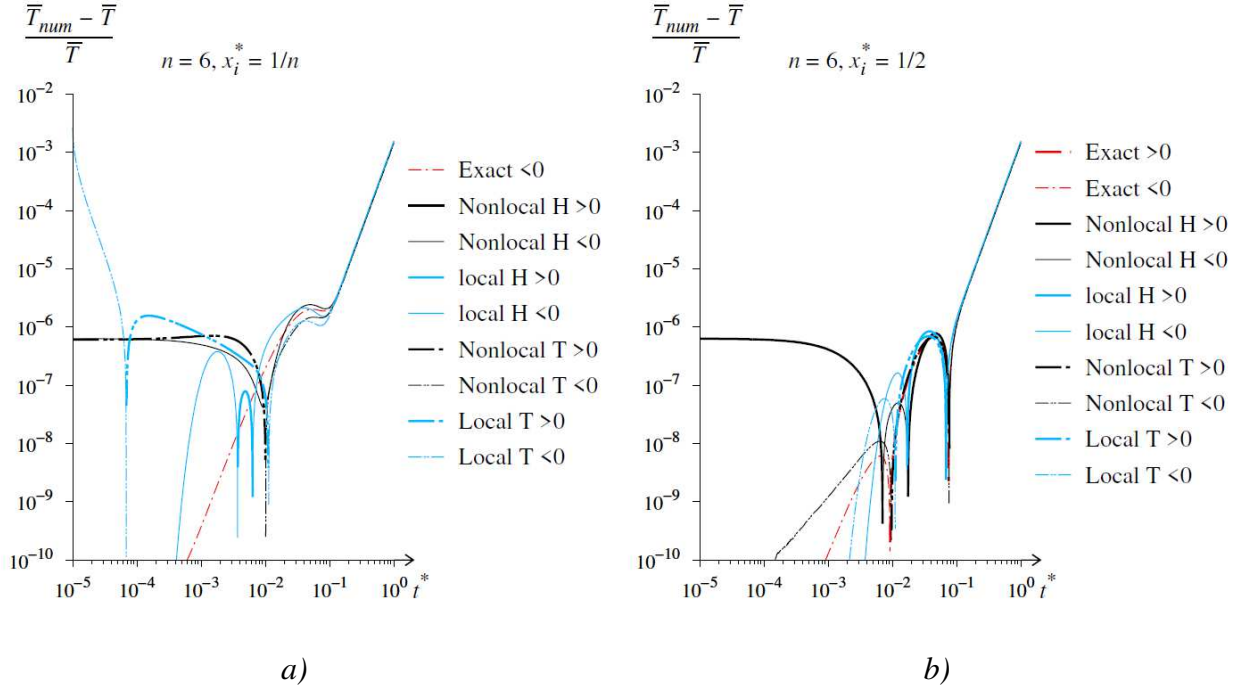
729 leading to solve the node temperatures of next time step \bar{T}_i^{j+1} with the following
730 system of $n\delta/2$ equations.

$$\begin{aligned}
& -(n\delta)^2 \left(\frac{1}{2} + \frac{l_c^{*2}}{\Delta t^*}\right)\bar{T}_{i-1}^{j+1} + \left[\frac{1}{\Delta t^*} + 2\left(\frac{1}{2} + \frac{l_c^{*2}}{\Delta t^*}\right)(n\delta)^2\right]\bar{T}_i^{j+1} - (n\delta)^2 \left[\frac{1}{2} + \frac{l_c^{*2}}{\Delta t^*}\right]\bar{T}_{i+1}^{j+1} \\
& = (n\delta)^2 \left(\frac{1}{2} - \frac{l_c^{*2}}{\Delta t^*}\right)\bar{T}_{i-1}^j + \left[\frac{1}{\Delta t^*} - 2\left(\frac{1}{2} - \frac{l_c^{*2}}{\Delta t^*}\right)(n\delta)^2\right]\bar{T}_i^j + (n\delta)^2 \left(\frac{1}{2} - \frac{l_c^{*2}}{\Delta t^*}\right)\bar{T}_{i+1}^j
\end{aligned} \tag{50}$$

731

732 The maximum relative differences of the numerical results with analytical ones are
733 obtained with Heaviside and trapezoidal initial conditions. As shown in Fig. 14, the
734 relative differences does not exceed 10^{-3} , and are around 10^{-6} or lower the this value
735 for the main diffusion period, i.e. from $t^*=10^{-4}$ to $t^*=7.10^{-1}$. These numerical results, in
736 very good accordance with the analytical ones, allow to validate the presented
737 analytical formulations.

738



739 *Fig. 14 : Relative differences in temperature between numerical and analytical results*
 740 *of the lattice model used as reference (named as “exact”) and local or nonlocal*
 741 *continualized model*
 742 *– a) at node 1 or n–1*
 743 *– b) at the mid length, i.e. at node n/2.*
 744
 745

746 **Appendix C: Discontinuity of nonlocal diffusion model at the boundaries**

747

748 Integration of the nonlocal diffusion equation defined in Eq. (2) over the region Ω ,
 749 close to the boundary, at the first extremity located at $x = 0$ such as $(-h \leq x^* \leq +h, \text{ for}$
 750 $0 \leq t \leq \Gamma)$, leads to:

$$\int_{-h}^{+h} [\bar{T}(x^*, \Gamma) - \bar{T}(x^*, 0)] dx - \int_0^\Gamma \left[\left(\alpha \bar{T}' + l_c^2 \bar{T}'' \right) \right]_{-h}^{+h} dt = 0 \quad (51)$$

751 When $h \rightarrow 0$, the first integral tends toward 0 and as consequence:

$$\int_0^\Gamma \left[\left(\alpha \bar{T}' + l_c^2 \bar{T}'' \right) \right]_{\ll}^{\gg} dt = 0 \quad (52)$$

752 where the double bracket sign $\ll \gg$ designates the difference in value on both side of the
 753 discontinuity, i.e. at $x = 0^-$ and $x = 0^+$. Since the expression under the integral sign is a

754 continuous function of dimensionless time until Γ , the first condition at the boundary is
 755 obtained:

$$\alpha \bar{T}' + l_c^2 \bar{T}'' = \alpha \bar{T}' + l_c^2 \bar{T}'' = 0 \quad (53)$$

756 Unfortunately, \bar{T}' is unknown, and a second condition based on \bar{T} has to be defined.
 757 Integration over the region Ω of the nonlocal diffusion equation multiplied by x^* gives:

$$\int_{-h}^{+h} [\bar{T}(x^*, \Gamma) - \bar{T}(x^*, 0)] x^* dx^* - \int_0^\Gamma x \alpha \bar{T}' + x l_c^2 \bar{T}'' dt + \int_0^\Gamma \alpha \bar{T} + l_c^2 \bar{T}'' dt = 0 \quad (54)$$

758 When $h \rightarrow 0$, the first and second integral tend toward 0. Hence, the condition at the
 759 boundary is obtained:

$$\alpha \bar{T} + l_c^2 \bar{T}'' = \alpha \bar{T}' + l_c^2 \bar{T}'' = 0 \quad (55)$$

760 It should be noted that due to the symmetry of the diffusion problem, the same
 761 demonstration can be made at the opposite boundary, at the second extremity located
 762 at $x = L$ or $x^* = 1$ in Heaviside case.

763 Solving this first order differential equation, according to the initial conditions at both
 764 boundaries, i.e. $\bar{T}(0^+, 0) - \bar{T}(0^-, 0) = 1 = \bar{T}(L^-, 0) - \bar{T}(L^+, 0)$ according to Eq. (6),
 765 gives the temperature immediately to the inside boundary:

$$\bar{T}(0^+, t) = \exp\left(-\frac{\alpha t}{l_c^2}\right) = \bar{T}(L^-, t) \quad (56)$$

766 This solution fulfills as well the first condition at the boundary previously established
 767 in Eq. (53).

768

769

770 **References**

771

- 772 [1] A.D. Myshkis, *Mixed Functional Differential Equations*, (n.d.) 116.
- 773 [2] N. Challamel, C. Grazide, V. Picandet, A. Perrot, Y. Zhang, A nonlocal Fourier's law and its
774 application to the heat conduction of one-dimensional and two-dimensional thermal lattices,
775 *Comptes Rendus Mécanique*. 344 (2016) 388–401. <https://doi.org/10.1016/j.crme.2016.01.001>.
- 776 [3] M. Zingales, An exact thermodynamical model of power-law temperature time scaling, *Ann. Phys.*
777 365 (2016) 24–37. <https://doi.org/10.1016/j.aop.2015.08.014>.
- 778 [4] R.A. Guyer, J.A. Krumhansl, Solution of the Linearized Phonon Boltzmann Equation, *Phys. Rev.*
779 148 (1966) 766–778. <https://doi.org/10.1103/PhysRev.148.766>.
- 780 [5] R.A. Guyer, J.A. Krumhansl, Thermal Conductivity, Second Sound, and Phonon Hydrodynamic
781 Phenomena in Nonmetallic Crystals, *Phys. Rev.* 148 (1966) 778–788.
782 <https://doi.org/10.1103/PhysRev.148.778>.
- 783 [6] D. Jou, G. Lebon, J. Casas-Vázquez, *Extended Irreversible Thermodynamics*, 4th ed., Springer
784 Netherlands, 2010. <https://doi.org/10.1007/978-90-481-3074-0>.
- 785 [7] K.V. Zhukovsky, Exact solution of Guyer–Krumhansl type heat equation by operational method,
786 *Int. J. Heat Mass Transf.* 96 (2016) 132–144.
787 <https://doi.org/10.1016/j.ijheatmasstransfer.2016.01.005>.
- 788 [8] R. Kovács, Analytic solution of Guyer-Krumhansl equation for laser flash experiments, *Int. J. Heat*
789 *Mass Transf.* 127 (2018) 631–636. <https://doi.org/10.1016/j.ijheatmasstransfer.2018.06.082>.
- 790 [9] C. Cattaneo, Sulla Conduzione del Calore, *Atti Sem Mat Fis Univ Modena*. 3 (1948) 83–101.
- 791 [10] A.C. Eringen, On differential equations of nonlocal elasticity and solutions of screw dislocation
792 and surface waves, *J. Appl. Phys.* 54 (1983) 4703–4710. <https://doi.org/10.1063/1.332803>.
- 793 [11] G.I. Barenblatt, Iu.P. Zheltov, I.N. Kochina, Basic concepts in the theory of seepage of
794 homogeneous liquids in fissured rocks [strata], *J. Appl. Math. Mech.* 24 (1960) 1286–1303.
795 [https://doi.org/10.1016/0021-8928\(60\)90107-6](https://doi.org/10.1016/0021-8928(60)90107-6).
- 796 [12] T.W. Ting, Certain non-steady flows of second-order fluids, *Arch. Ration. Mech. Anal.* 14 (1963)
797 1–26. <https://doi.org/10.1007/BF00250690>.
- 798 [13] A. Sellitto, F.X. Alvarez, D. Jou, Geometrical dependence of thermal conductivity in elliptical and
799 rectangular nanowires, *Int. J. Heat Mass Transf.* 55 (2012) 3114–3120.
800 <https://doi.org/10.1016/j.ijheatmasstransfer.2012.02.045>.
- 801 [14] G.A. Maugin, On the thermomechanics of continuous media with diffusion and/or weak
802 nonlocality, *Arch. Appl. Mech.* 75 (2006) 723. <https://doi.org/10.1007/s00419-006-0062-4>.
- 803 [15] A. Sellitto, D. Jou, J. Bafaluy, Non-local effects in radial heat transport in silicon thin layers and
804 graphene sheets, *Proc. R. Soc. Math. Phys. Eng. Sci.* 468 (2012) 1217–1229.
805 <https://doi.org/10.1098/rspa.2011.0584>.
- 806 [16] D. Jou, V.A. Cimmelli, A. Sellitto, Nonlocal heat transport with phonons and electrons:
807 Application to metallic nanowires, *Int. J. Heat Mass Transf.* 55 (2012) 2338–2344.
808 <https://doi.org/10.1016/j.ijheatmasstransfer.2012.01.033>.
- 809 [17] D. Jou, A. Sellitto, F.X. Alvarez, Heat waves and phonon–wall collisions in nanowires, *Proc. R.*
810 *Soc. Math. Phys. Eng. Sci.* 467 (2011) 2520–2533. <https://doi.org/10.1098/rspa.2010.0645>.
- 811 [18] A. Berezovski, J. Engelbrecht, P. Ván, Weakly nonlocal thermoelasticity for microstructured
812 solids: microdeformation and microtemperature, *Arch. Appl. Mech.* 84 (2014) 1249–1261.
813 <https://doi.org/10.1007/s00419-014-0858-6>.

- 814 [19] S.P. Filopoulos, T.K. Papathanasiou, S.I. Markolefas, G.J. Tsamasphyros, Generalized
815 Thermoelastic Models for Linear Elastic Materials with Micro-Structure Part I: Enhanced Green–
816 Lindsay Model, *J. Therm. Stress.* 37 (2014) 624–641.
817 <https://doi.org/10.1080/01495739.2014.885325>.
- 818 [20] S.P. Filopoulos, T.K. Papathanasiou, S.I. Markolefas, G.J. Tsamasphyros, Generalized
819 Thermoelastic Models for Linear Elastic Materials with Micro-Structure Part II: Enhanced Lord–
820 Shulman Model, *J. Therm. Stress.* 37 (2014) 642–659.
821 <https://doi.org/10.1080/01495739.2014.885327>.
- 822 [21] T. Atanacković, S. Konjik, L. Oparnica, D. Zorica, The Cattaneo type space-time fractional heat
823 conduction equation, *Contin. Mech. Thermodyn.* 24 (2012) 293–311.
824 <https://doi.org/10.1007/s00161-011-0199-4>.
- 825 [22] G. Lebon, M. Grmela, Weakly nonlocal heat conduction in rigid solids, *Phys. Lett. A.* 214 (1996)
826 184–188. [https://doi.org/10.1016/0375-9601\(96\)00159-4](https://doi.org/10.1016/0375-9601(96)00159-4).
- 827 [23] R. Kovács, P. Ván, Generalized heat conduction in heat pulse experiments, *Int. J. Heat Mass*
828 *Transf.* 83 (2015) 613–620. <https://doi.org/10.1016/j.ijheatmasstransfer.2014.12.045>.
- 829 [24] S. Chandrasekhar, Stochastic Problems in Physics and Astronomy, *Rev. Mod. Phys.* 15 (1943) 1–
830 89. <https://doi.org/10.1103/RevModPhys.15.1>.
- 831 [25] H.D. Weymann, Finite Speed of Propagation in Heat Conduction, Diffusion, and Viscous Shear
832 Motion, *Am. J. Phys.* 35 (1967) 488–496. <https://doi.org/10.1119/1.1974155>.
- 833 [26] Y. Taitel, On the parabolic, hyperbolic and discrete formulation of the heat conduction equation,
834 *Int. J. Heat Mass Transf.* 15 (1972) 369–371. [https://doi.org/10.1016/0017-9310\(72\)90085-3](https://doi.org/10.1016/0017-9310(72)90085-3).
- 835 [27] S.L. Sobolev, Discrete model for transfer processes, *Phys. Lett. A.* 163 (1992) 101–103.
836 [https://doi.org/10.1016/0375-9601\(92\)90169-M](https://doi.org/10.1016/0375-9601(92)90169-M).
- 837 [28] S.L. Sobolev, Nonlocal diffusion models: Application to rapid solidification of binary mixtures,
838 *Int. J. Heat Mass Transf.* 71 (2014) 295–302.
839 <https://doi.org/10.1016/j.ijheatmasstransfer.2013.12.048>.
- 840 [29] S.L. Sobolev, I.V. Kudinov, Heat conduction across 1D nano film: Local thermal conductivity and
841 extrapolation length, *Int. J. Therm. Sci.* 159 (2021) 106632.
842 <https://doi.org/10.1016/j.ijthermalsci.2020.106632>.
- 843 [30] N. Challamel, C.M. Wang, I. Elishakoff, Nonlocal or gradient elasticity macroscopic models: A
844 question of concentrated or distributed microstructure, *Mech. Res. Commun.* 71 (2016) 25–31.
845 <https://doi.org/10.1016/j.mechrescom.2015.11.006>.
- 846 [31] J. Crank, P. Nicolson, A practical method for numerical evaluation of solutions of partial
847 differential equations of the heat-conduction type, *Math. Proc. Camb. Philos. Soc.* 43 (1947) 50–
848 67. <https://doi.org/10.1017/S0305004100023197>.
- 849 [32] J.G. Charney, R. Fjørtoft, J. von Neumann, Numerical Integration of the Barotropic Vorticity
850 Equation, in: R.S. Lindzen, E.N. Lorenz, G.W. Platzman (Eds.), *Atmosphere — Chall. Sci. Jule*
851 *Gregory Charney*, American Meteorological Society, Boston, MA, 1990: pp. 267–284.
852 https://doi.org/10.1007/978-1-944970-35-2_15.
- 853 [33] L. Collatz, *The Numerical Treatment of Differential Equations*, Springer Science & Business
854 Media, 2012.
- 855 [34] B. Gustafsson, H.-O. Kreiss, J. Oliger, *Time Dependent Problems and Difference Methods*, John
856 Wiley & Sons, 1995.
- 857 [35] S. Goldberg, *Introduction to Difference Equations: With Illustrative Examples from Economics,*
858 *Psychology, and Sociology*, Courier Corporation, 1958.
- 859 [36] N. Challamel, V. Picandet, B. Collet, T. Michelitsch, I. Elishakoff, C.M. Wang, Revisiting finite
860 difference and finite element methods applied to structural mechanics within enriched continua,
861 *Eur. J. Mech. - ASolids.* 53 (2015) 107–120. <https://doi.org/10.1016/j.euromechsol.2015.03.003>.

- 862 [37] T.W. Körner, *Fourier Analysis*, Cambridge University Press, Cambridge, 1988.
863 <https://doi.org/10.1017/CBO9781107049949>.
- 864 [38] Y. Belmoujahid, N. Challamel, V. Picandet, Propagation locale et non-locale de la chaleur dans un
865 barreau hétérogène, *Acad. J. Civ. Eng.* 35 (2017) 160–163. <https://doi.org/10.26168/ajce.35.1.39>.
- 866 [39] H.S. Carslaw, *Introduction to the theory of Fourier's series and integrals*, London, Macmillan and
867 co., limited, 1921.
- 868 [40] P.G. Kevrekidis, I.G. Kevrekidis, A.R. Bishop, E.S. Titi, Continuum approach to discreteness,
869 *Phys. Rev. E.* 65 (2002) 046613. <https://doi.org/10.1103/PhysRevE.65.046613>.
- 870 [41] I.V. Andrianov, J. Awrejcewicz, D. Weichert, Improved Continuous Models for Discrete Media,
871 *Math. Probl. Eng.* 2010 (2010) 1–35. <https://doi.org/10.1155/2010/986242>.
- 872 [42] M.A. Collins, A quasicontinuum approximation for solitons in an atomic chain, *Chem. Phys. Lett.*
873 77 (1981) 342–347. [https://doi.org/10.1016/0009-2614\(81\)80161-3](https://doi.org/10.1016/0009-2614(81)80161-3).
- 874 [43] N. Triantafyllidis, S. Bardenhagen, On higher order gradient continuum theories in 1-D nonlinear
875 elasticity. Derivation from and comparison to the corresponding discrete models, *J. Elast.* 33
876 (1993) 259–293.
- 877 [44] P. Rosenau, Dynamics of nonlinear mass-spring chains near the continuum limit, *Phys. Lett. A.*
878 118 (1986) 222–227. [https://doi.org/10.1016/0375-9601\(86\)90170-2](https://doi.org/10.1016/0375-9601(86)90170-2).
- 879 [45] J.A.D. Wattis, Quasi-continuum approximations to lattice equations arising from the discrete
880 nonlinear telegraph equation, *J. Phys. Math. Gen.* 33 (2000) 5925–5944.
881 <https://doi.org/10.1088/0305-4470/33/33/311>.
- 882 [46] M. Charlotte, L. Truskinovsky, Lattice dynamics from a continuum viewpoint, *J. Mech. Phys.*
883 *Solids.* 60 (2012) 1508–1544. <https://doi.org/10.1016/j.jmps.2012.03.004>.
- 884 [47] N. Challamel, C.M. Wang, I. Elishakoff, Discrete systems behave as nonlocal structural elements:
885 Bending, buckling and vibration analysis, *Eur. J. Mech. - ASolids.* 44 (2014) 125–135.
886 <https://doi.org/10.1016/j.euromechsol.2013.10.007>.
- 887 [48] N. Challamel, V. Picandet, G. Pijaudier-Cabot, From discrete to nonlocal continuum damage
888 mechanics: Analysis of a lattice system in bending using a continualized approach, *Int. J. Damage*
889 *Mech.* (2014a). <https://doi.org/10.1177/1056789514560913>.
- 890 [49] V. Picandet, N. Challamel, Bending of an elastoplastic Hencky bar-chain: from discrete to
891 nonlocal continuous beam models, *Meccanica.* 53 (2018) 3083–3104.
892 <https://doi.org/10.1007/s11012-018-0862-y>.
- 893 [50] V. Picandet, B. Hérisson, N. Challamel, A. Perrot, On the failure of a discrete axial chain using a
894 continualized nonlocal Continuum Damage Mechanics approach, *Int. J. Numer. Anal. Methods*
895 *Geomech.* (2016). <https://onlinelibrary.wiley.com/doi/abs/10.1002/nag.2412> (accessed September
896 30, 2019).
- 897 [51] W.H. Press, B.P. Flannery, S.A. Teukolsky, W.T. Vetterling, *Numerical recipes in C: the art of*
898 *scientific computing*, Cambridge University Press, USA, 1988.
- 899